

III CHAPTER : THERMODYNAMICS OF HYDROGEN IN METALS

III.1	Phase diagrams and pressure-composition isotherms	2
III.2	Heat of solution and heat of formation	14
III.3	Mean-field theory of the lattice-gas	23
III.3.1	Plateau dissociation pressures	33
III.3.2	Determination of the H-H interaction parameter	34
III.3.3	Coexistence curve	35
III.3.4	Inclusion of thermal and steric effects	40
III.4	Heat of formation of alloys	44
III.5	Semi-empirical models	48
III.5.1	The Miedema model	48
III.5.2	The semi-empirical band structure model	49
III.6	References	52

III.1 PHASE DIAGRAMS AND PRESSURE-COMPOSITION ISOTHERMS

One of the first measurements needed to characterise a metal-hydride system is to measure its solubility isotherms or pressure-composition isotherms. In these experiments one measures the concentration of hydrogen inside the sample (by measuring its weight, for example) as a function of the hydrogen gas pressure around the sample. A schematic representation of the apparatus used by Feenstra et al¹ to investigate the PdH_x system is shown in Fig. III.1.

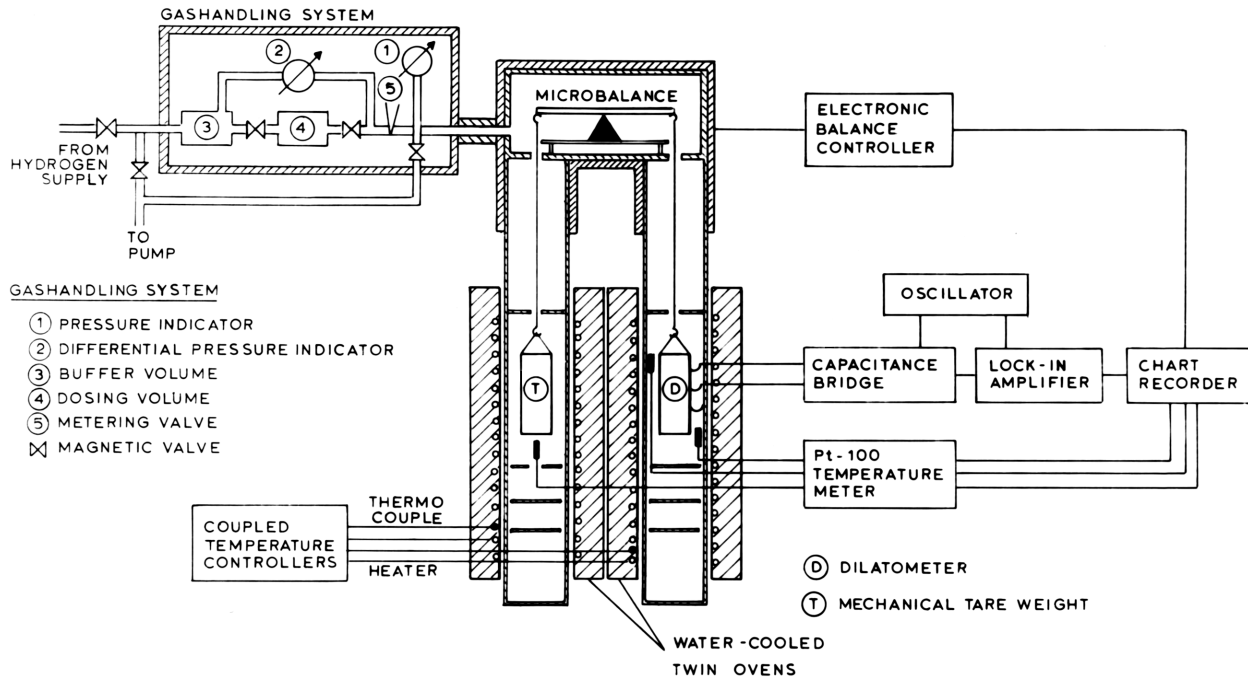


Fig. III.1: Experimental apparatus used by Feenstra et al.¹ for measurements of solubility isotherms. The sensitivity of the balance is 1 μg . The sample is placed in a dilatometer to measure additionally the lattice expansion during hydrogen absorption.

The sample is usually in the form of foils in order to avoid long times to reach equilibrium (thickness 10 μm - 100 μm). The procedure is as follows. First, the reaction chamber is evacuated. Then hydrogen gas is added to reach a pre-set pressure and maintain it until the concentration inside the sample has reached its equilibrium value. The pressure is increased and the whole procedure is repeated at constant temperature. Solubility isotherms for PdH_x, NbH_x, TaH_x and VH_x, are shown in Fig. III.2, Fig. III.4 and Fig. III.6. All the isotherms have approximately the same shape but in the case of NbH_x and PdH_x there exists a set of isotherms with a well defined plateau. As in the case of the van der Waals equation of state, these plateaux indicate the presence of two coexisting phases: a dilute metal-hydride MH_x phase (α -phase) and a concentrated phase (α' -phase). The corresponding T versus x phase diagrams are indicated in Fig. III.3, Fig. III.5, and Fig. III.7.

In the case of PdH_x and NbH_x it is quite evident that a two-phase region exists. For TaH_x and VH_x additional experimental information is required to draw the phase boundaries.

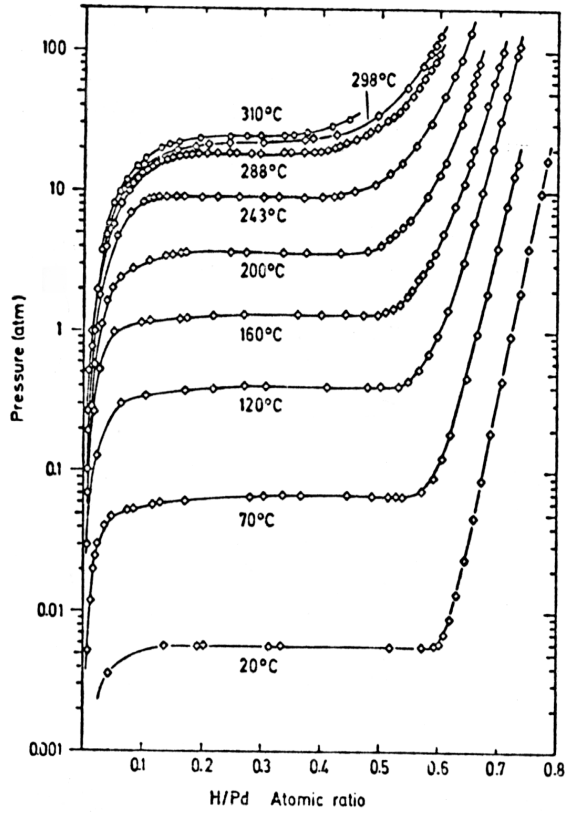


Fig. III.2: Pressure-composition isotherms for H in Pd (see Frieske and Wicke², and Gillespie and Galstaun³)

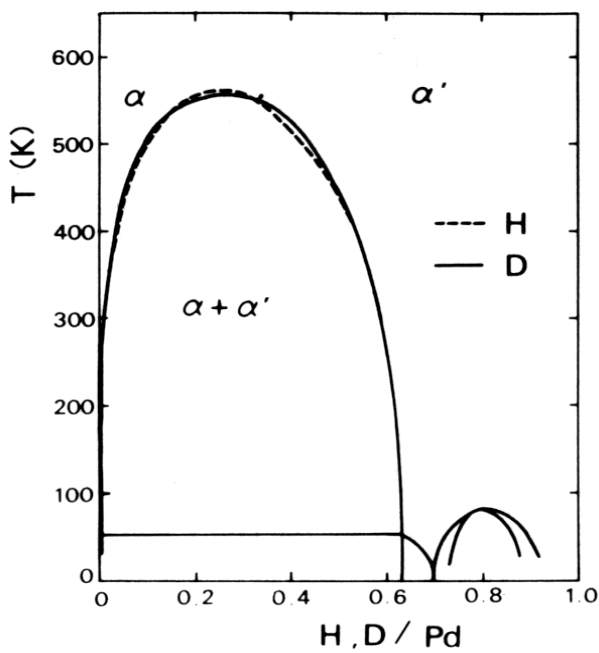


Fig. III.3: Details of the phase diagram of PdH_x and PdD_x . In this system isotope effects are rather small in sharp contrast to, for example, the VH_x system. (Frieske and Wicke², Wicke and Blaurock⁴, and Bond and Ross⁵.)

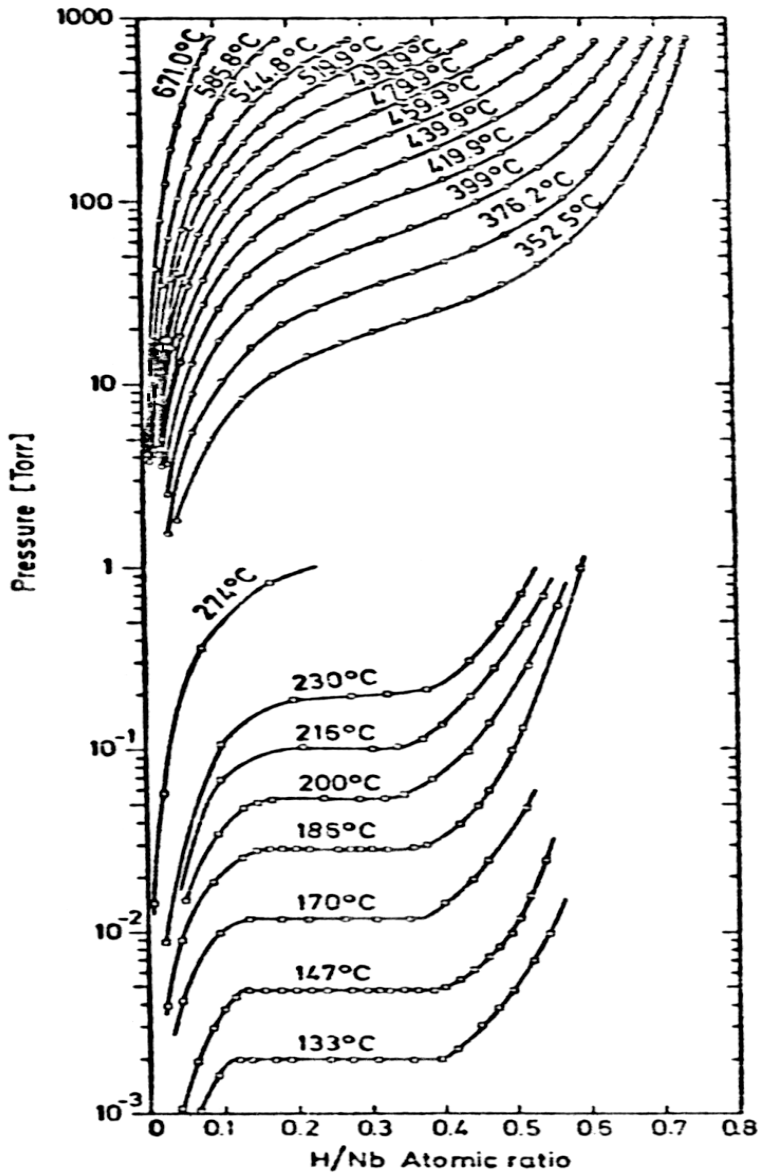


Fig.III.4: Pressure-composition isotherms for H in Nb Veleckis, Pryde and Titcomb⁶.

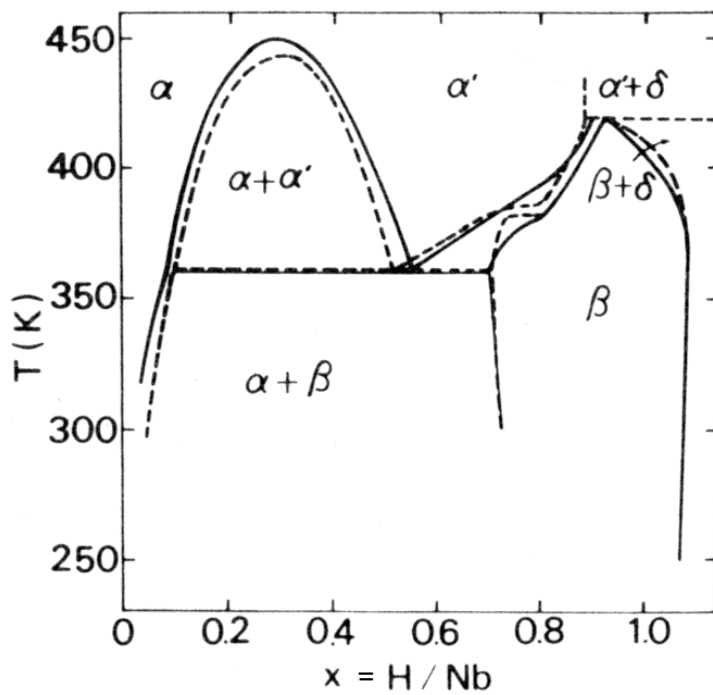


Fig.III.5: Details of the phase diagram of NbH_x . [Schober and Wenzl]. The full line is a calculation by Kuji and Oates⁷.

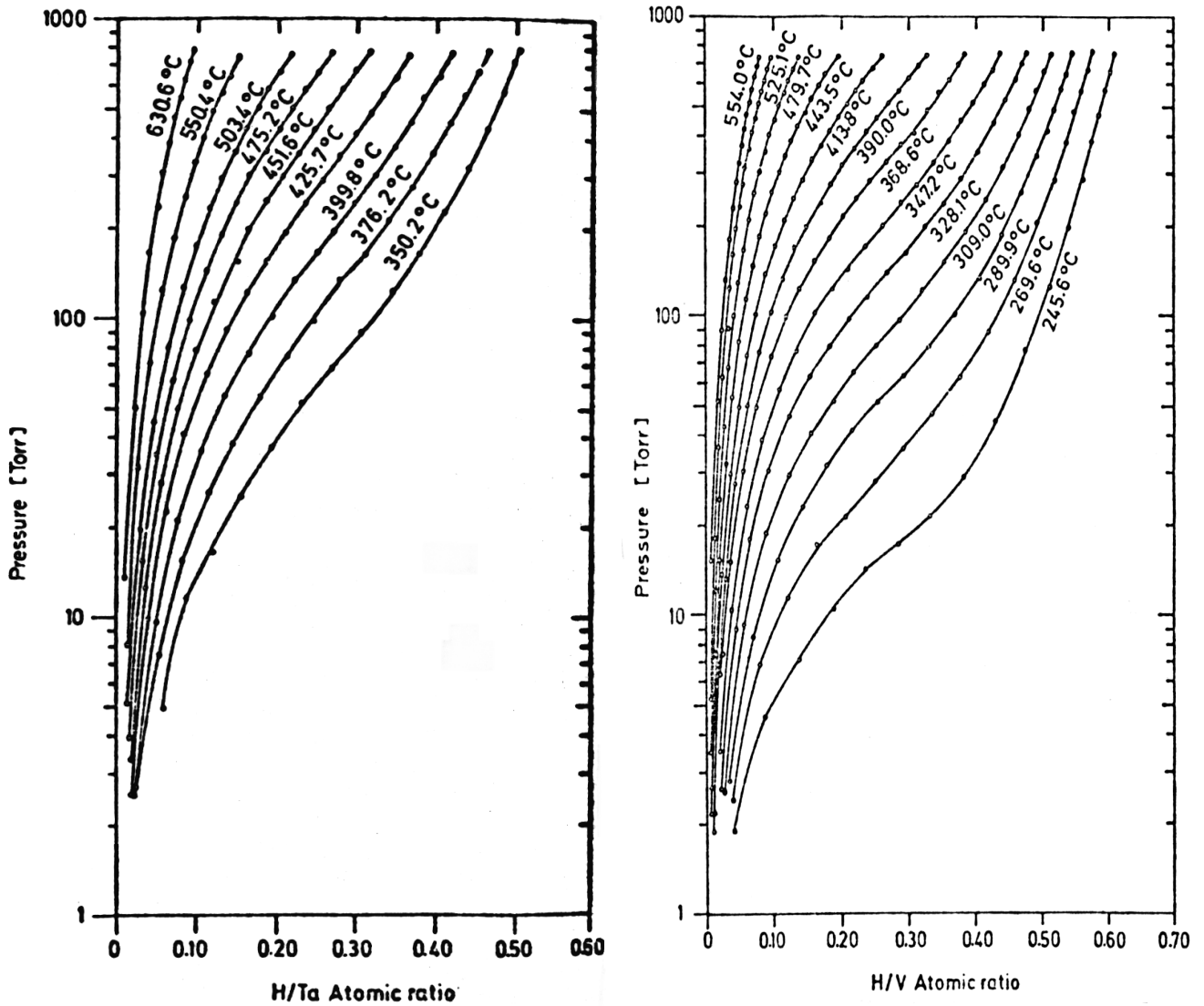


Fig. III.6: Pressure-composition isotherms for H in Ta (left) and for H in V (right) according to Veleckis⁸.

The most commonly used methods for detecting and measuring different phases are

- X-ray measurements of lattice constants.
- Electron microscopy (TEM: Transmission Electron Microscopy)
- Differential thermal analysis

As these techniques are well known, we shall just give a few examples of the type of data which can be obtained from such experiments (see Fig. III.7, Fig. III.9, and Fig. III.10).

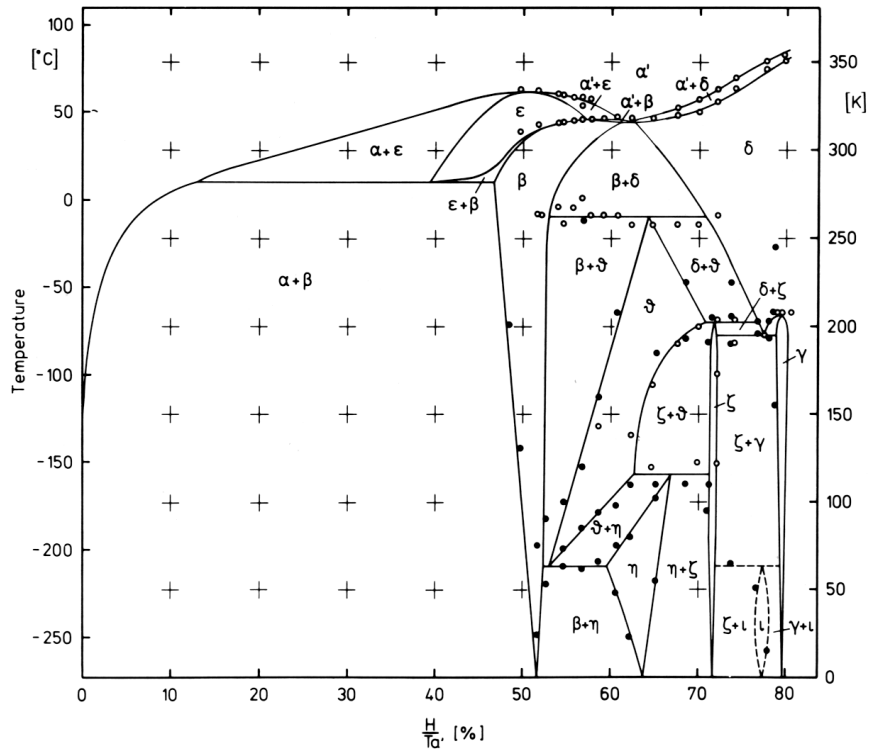


Fig. III.7: The TaH_x phase diagram according to Schober⁹. α and α' are disordered BCC solutions of H in Ta. ϵ is a tetragonal phase and β , δ , ζ and γ are orthorhombic. The α' - β is a disorder-order transformation for the H atoms.

A typical example of a TEM-micrograph is shown in Fig. III.9 for a $PdH_{0.7}$ sample in the α - α' (α - β) mixed phase. The little islands with smooth contours are so-called **coherent** precipitations of α -phase in the α' -matrix, while the dark and sharp regions correspond to **incoherent** precipitates of α -phase in α' (coherent means that the topology of the lattice is not destroyed while incoherent implies that abrupt changes are occurring at the boundary of the precipitates). The formation of coherent and incoherent precipitates shall be discussed later in connection with the form of phase diagrams of MH_x systems.

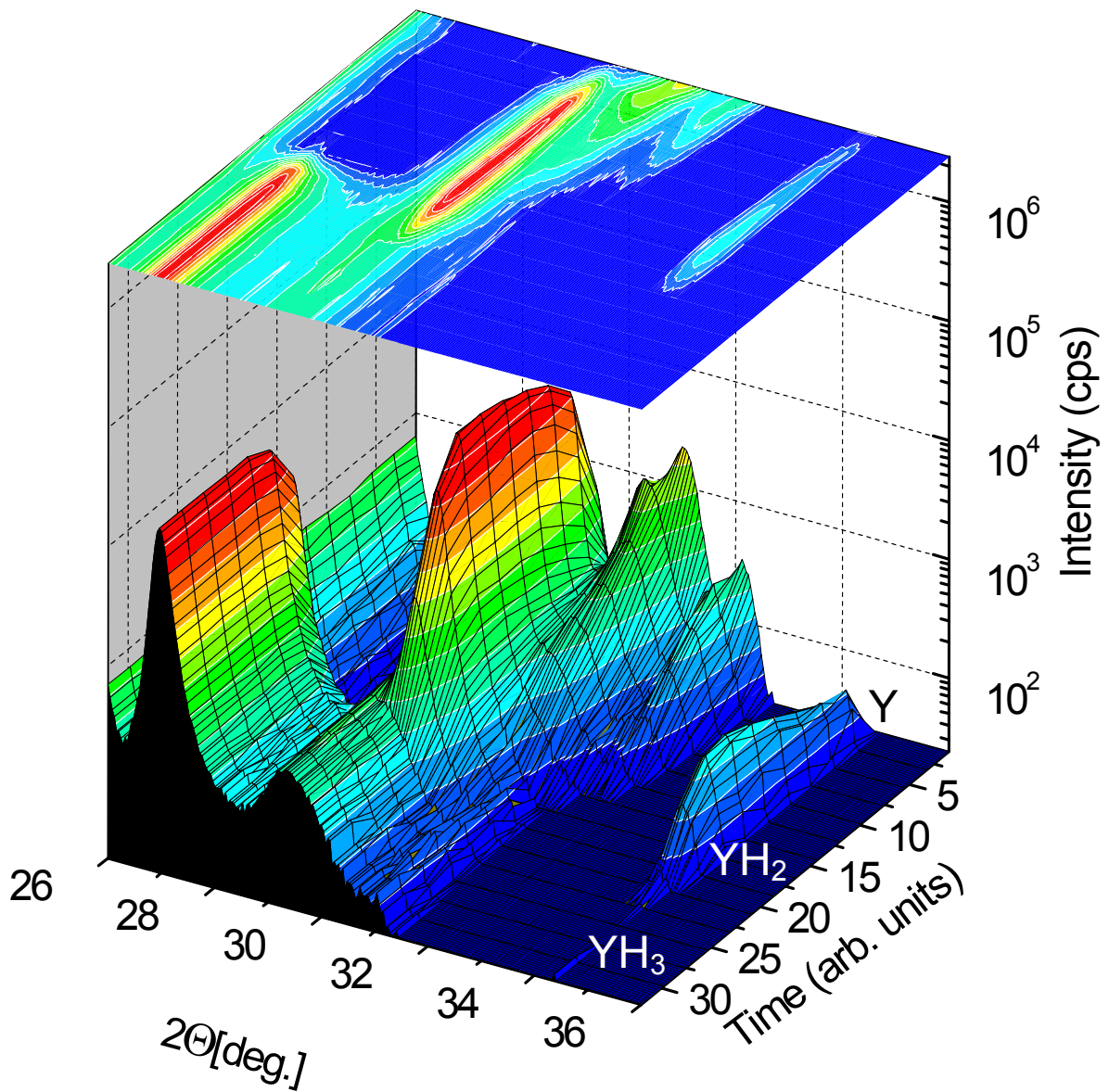


Fig. III.8: Time evolution of the X-ray scattering intensity of an yttrium film during hydrogen absorption at room temperature. For clarity the time axis starts at the back of the plot. Time $t=0$ corresponds to the moment when hydrogen starts to be absorbed by the film. Clearly visible is the variation of the peak intensity as a function of hydrogen concentration. This is due to a change in crystal structure. From detailed X-ray measurements one knows that YH_x changes from hcp at low concentration, to fcc in the dihydride phase YH_2 and back to hcp in the trihydride YH_3 . As the peaks occur at lower angles one concludes that YH_3 has larger lattice parameters than pure Y.

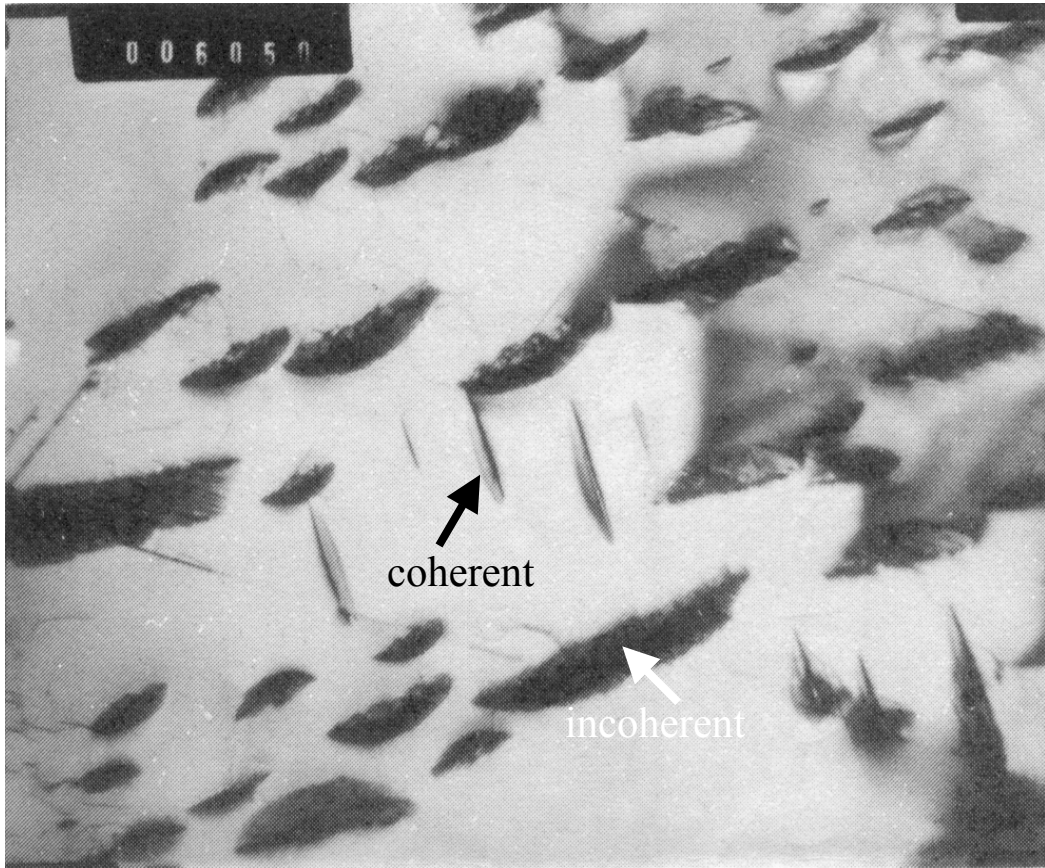
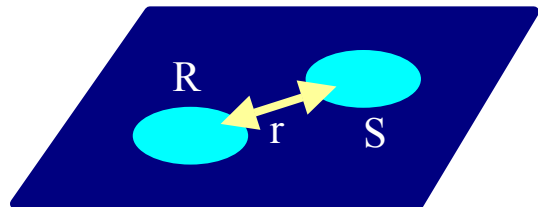


Fig. III.9: TEM micrograph of α - α' PdH_x with $x=0.6$ at $T= 86$ K [from King and Manchester¹⁰].

In DTA one measures the temperature difference ΔT between the sample under investigation (S) and a reference sample (R) in thermal contact with each other. $\Delta T=(T_S-T_R)$ is measured as function of time, with T (the temperature of the oven) scanned linearly in time. If the sample undergoes a phase transformation, there is a net heat flow between S and R. If the thermal resistivity of the heat-link is r , then the heat flow dQ/dt is

$$\frac{dQ}{dt} = \frac{\Delta T}{r}$$



This makes it possible to measure latent heats at a phase transition. For an example see Fig. III.10.

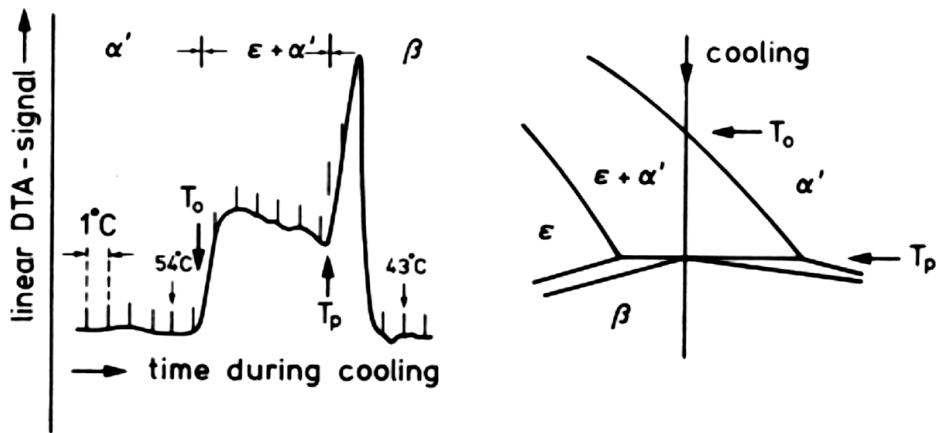


Fig. III.10: Differential Thermal Analysis (DTA) of TaH_x with $x=0.59$ recorded during slow cooling down (0.1 K/min). The path in the phase diagram is shown in the right panel. [Schober and Wenzl¹¹, see also Fig. III.7].

It is a formidable task to calculate all the details of a phase diagram such as the one shown in Fig. III.7 for TaH_x . One can nevertheless try to find an adequate description for some parts of the phase diagrams. Let us, therefore, come back to Fig. III.3 and Fig. III.5 and try to find some general characteristics. For this it is instructive to focus our attention onto Fig. III.5, the phase diagram of NbH_x and to compare it to the phase diagram of a normal gas-liquid-solid phase diagram (see Fig. III.11). One sees from Fig. III.11 that if the T-V phase diagram is replotted as T-(1/V) diagram we obtain a phase diagram of the same topology as that of NbH_x and PdH_x .

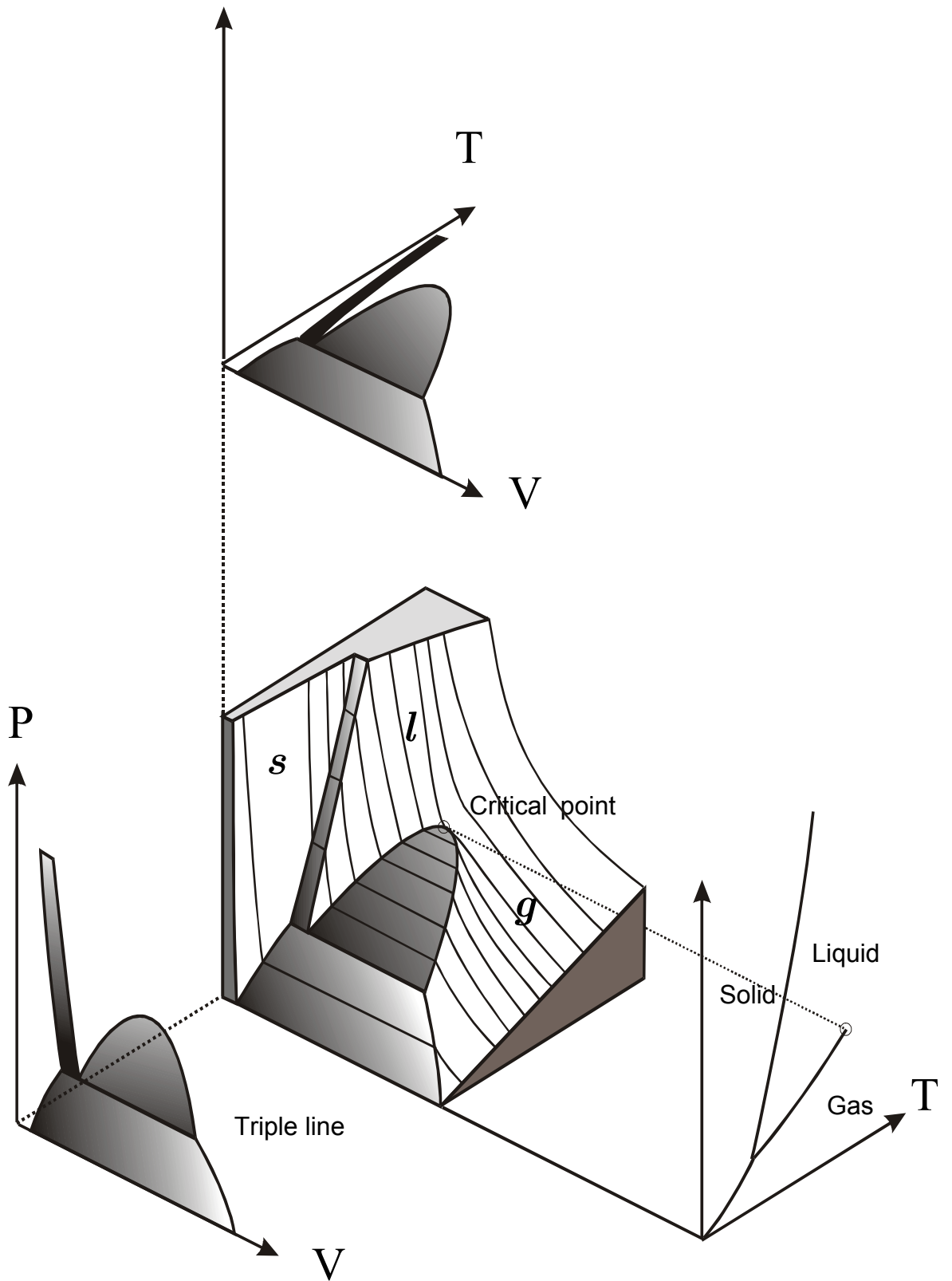


Fig. III.11: Phase diagram of a substance that contracts on freezing. When the top panel is plotted as T versus $1/V$, which is similar to a concentration, one obtains a phase diagram that is similar to the one shown in Fig.III.5 for NbH_x .

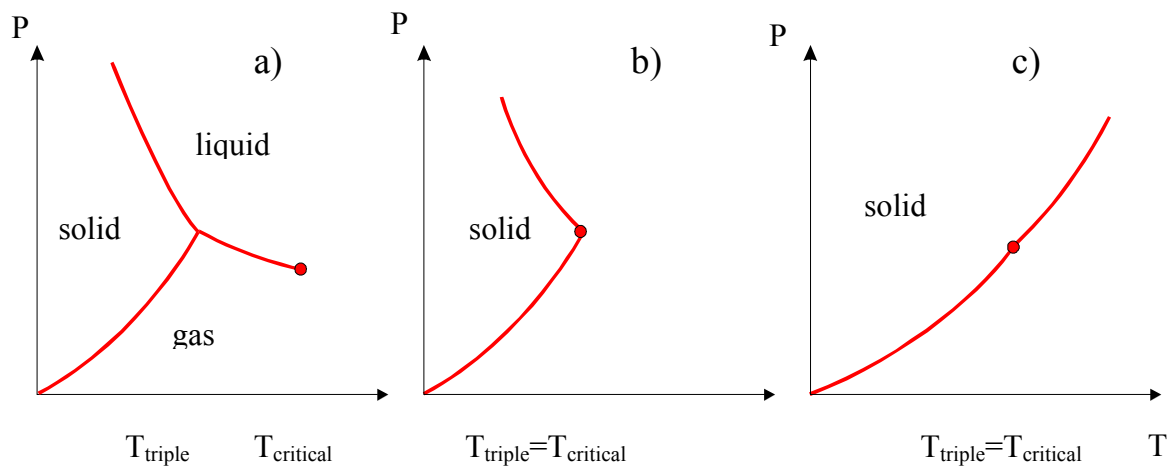


Fig. III.12: Pressure-temperature phase diagram of a substance which expands on freezing (left), of a substance which expands but with a triple point equal to the critical point (middle) and a normal substance which contracts on freezing but with $T_{\text{triple}}=T_c$.

Let us now investigate the case of a substance which expands on freezing (for example ice, Ge, Be, Si, Ce). For such substances we have the situation shown in Fig. III.12a. A limiting case of the situation a) is shown in Fig. III.12b. We shall show now that an ice-like substance with $T_t=T_c$ (triple point = critical point) has a phase diagram which is topologically equivalent to the two-phase region of the phase diagrams of TaH_x and VH_x . For this we just need to look at Fig. III.14.

This remarkable analogy of the phase diagram of M-H systems with those of one component systems has been noted by Hill¹², Torrey¹³ and developed by Alefeld¹⁴. In section III.3 we shall give a “one component” description of MH_x systems and introduce the notion of **lattice gas**.

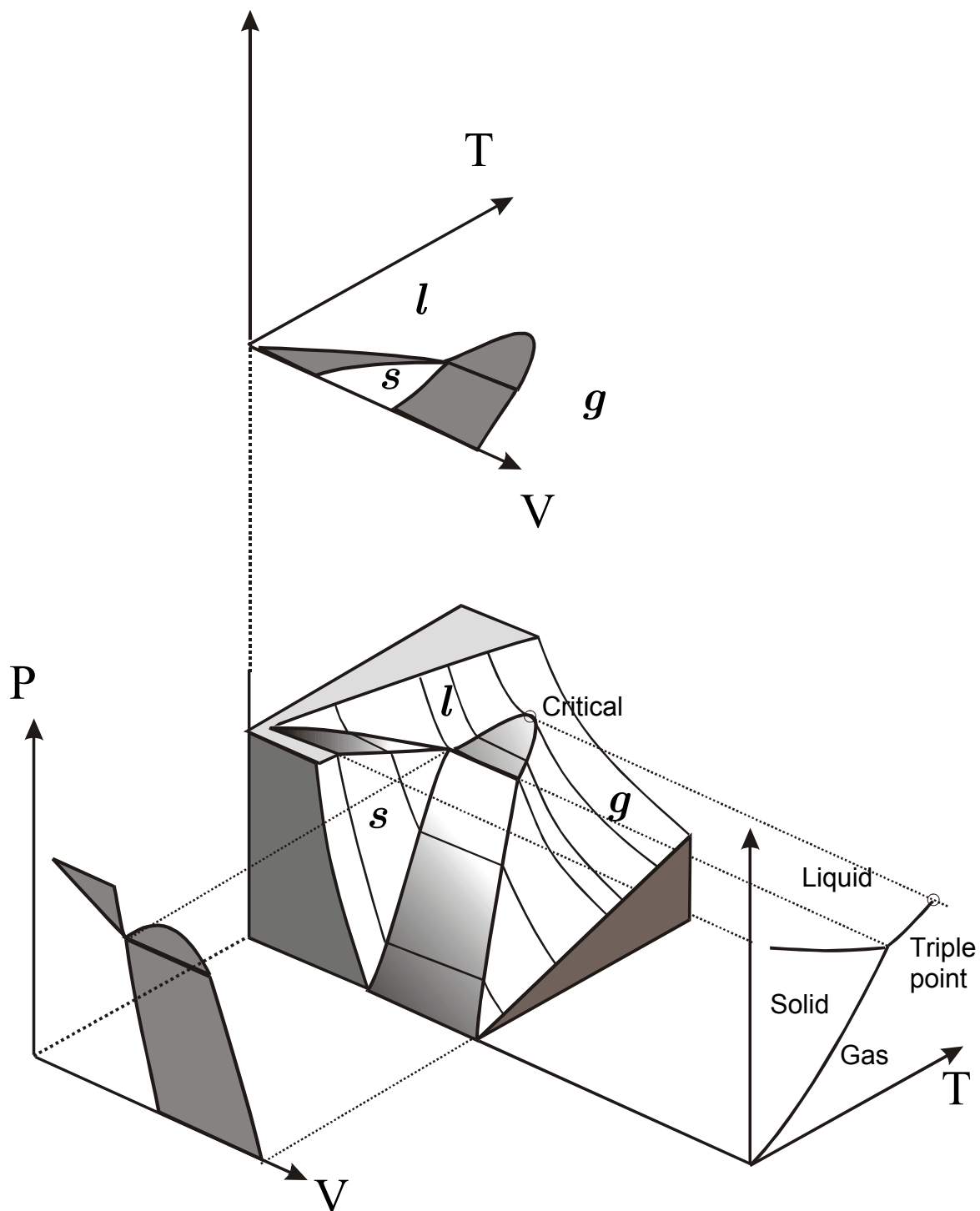


Fig. III.13: Phase diagram of a substance that expands on freezing. When the top panel is plotted as T versus $1/V$, which is similar to a concentration, one obtains a phase diagram that is similar to that shown in Fig. III.7 for the VH_x system if one assumes that the triple point coincides with the critical point, i.e. $T_{\text{triple}}=T_c$. This is explicitly shown in Fig. III.14.

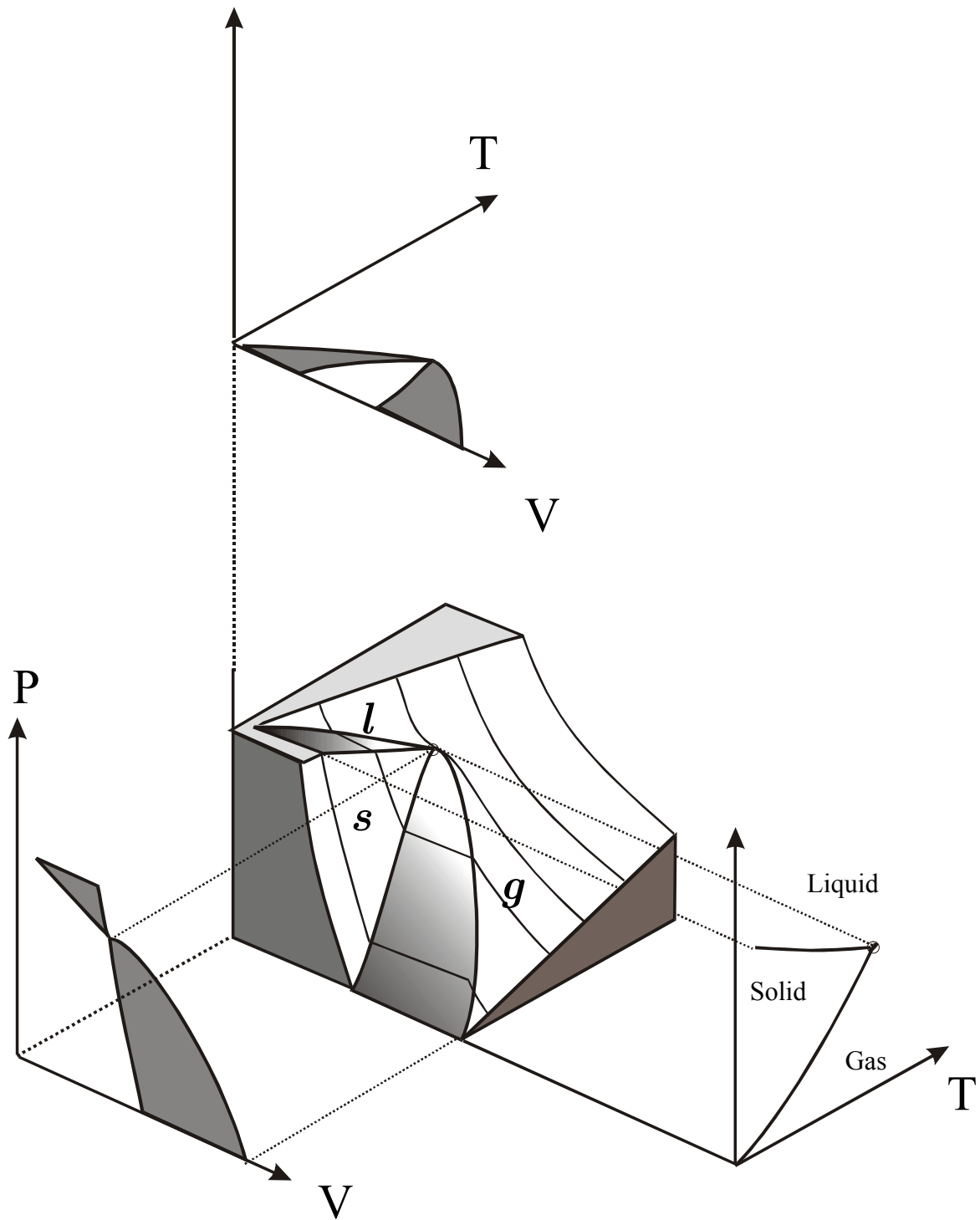


Fig. III.14: Phase diagram of a substance which expands on freezing and for which the triple point coincides with the critical point, i.e. $T_{\text{triple}}=T_c$. This is an extreme case of the phase diagram shown in Fig. III.13.

III.2 HEAT OF SOLUTION AND HEAT OF FORMATION

Another fundamental characteristics of a metal-hydride system is its heat of formation ΔH , i.e. the amount of heat absorbed or liberated during hydrogen absorption by the metallic host. ΔH determines essentially the stability of metal hydrides because it is directly related to the dissociation pressure p_{dis} via the van 't Hoff relation (to be derived later)

$$\frac{1}{2} \ln p_{dis} = \frac{\Delta H}{RT} - \frac{\Delta S}{R} \quad (\text{III.1})$$

where the entropy of formation ΔS is approximately constant for all metal-hydrogen systems as it arises mainly from the entropy loss of gaseous hydrogen during hydrogen uptake by the metal (see below).

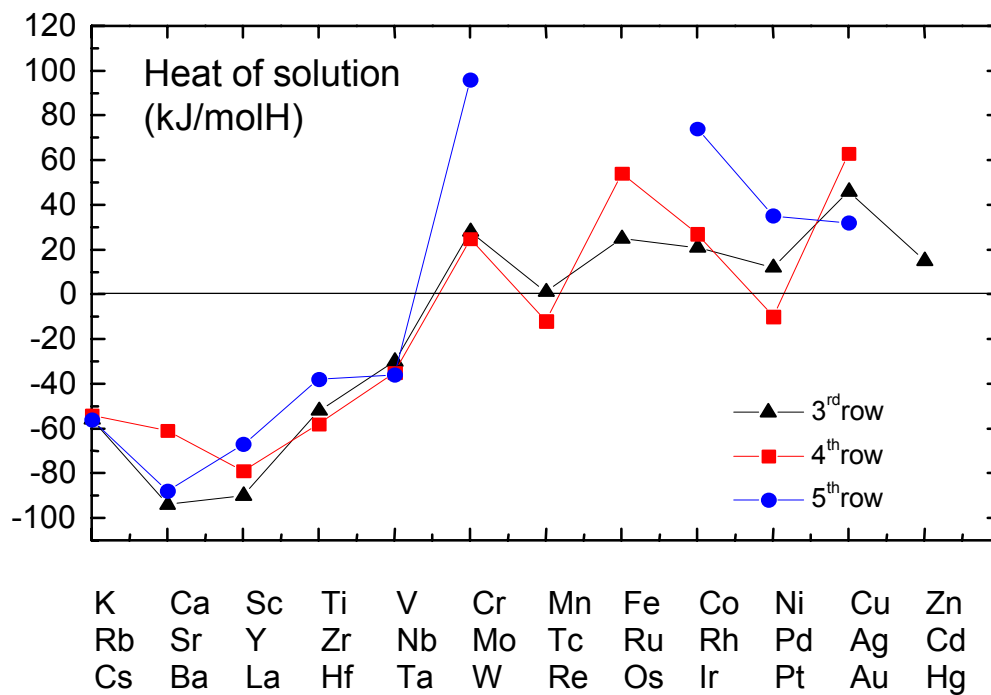


Fig. III.15: Heat of solution of hydrogen in the rows of the periodic system which contains the 3d, 4d and 5d elements. For references see Griessen and Riesters¹⁵.

Table III.1: Heat of solution of hydrogen in the elements of the periodic system .

Element	Enthalpy of solution (kJ/molH)	Enthalpy of solution (eV/atom)
He	--	--
Li	-51	-0.528
Be	-2	-0.02
B	-4	-0.041
C	--	--
N	--	--
O	--	--
F	--	--
Ne	--	--
Na	2	0.02
Mg	21	0.217
Al	60	0.621
Si	180	1.865
P	--	--
S	--	--
Cl	--	--
Ar	--	--
K	0	0
Ca	-94	-0.974
Sc	-90	-0.932
Ti	-52	-0.538
V	-30	-0.31
Cr	28	0.29
Mn	1	0.01
Fe	25	0.259
Co	21	0.217
Ni	12	0.124
Cu	46	0.476
Zn	15	0.155
Ga	--	--
Ge	221	2.29
As	--	--
Se	35	0.362
Br	--	--
Kr	--	--
Rb	-54	-0.559
Sr	-61	-0.632
Y	-79	-0.818
Zr	-58	-0.601
Nb	-35	-0.362
Mo	25	0.259
Tc	-12	-0.124
Ru	54	0.559
Rh	27	0.279
Pd	-10	-0.103

Element	Enthalpy of solution (kJ/molH)	Enthalpy of solution (eV/atom)
Ag	63	0.652
Cd	-94	-0.974
In	--	--
Sn	125	1.295
Sb	--	--
Te	-84	-0.87
I	--	--
Xe	--	--
Cs	-56	-0.58
Ba	-88	-0.912
La	-67	-0.694
Ce	-74	-0.766
Pr	-68	-0.704
Nd	-50	-0.518
Pm	--	--
Sm	-70	-0.725
Eu	--	--
Gd	-69	-0.715
Tb	-78	-0.808
Dy	-79	-0.818
Ho	--	--
Er	--	--
Tm	--	--
Yb	--	--
Lu	-79	-0.818
Hf	-38	-0.393
Ta	-36	-0.373
W	96	0.994
Re	--	--
Os	--	--
Ir	74	0.766
Pt	35	0.362
Au	32	0.331
Hg	--	--
Tl	--	--
Pb	62	0.642
Bi	--	--
Po	--	--
At	--	--
Rn	--	--
Fr	--	--
Ra	--	--
Ac	--	--
Th	-40	-0.414
Pa	--	--
U	7	0.072

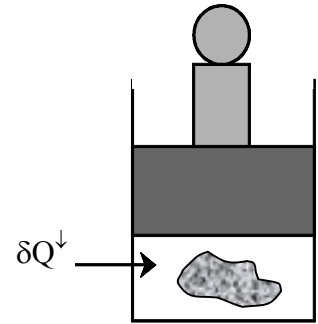
The purpose of this section is to introduce the concept of heat of formation and to provide the reader with up-to-date data on ΔH . The treatment is phenomenological. A more microscopic description shall be presented in the context of the electronic structure of metal-hydrides in later chapters.

As can be seen from Fig. III.15, the dissolution of hydrogen in a metal can be exothermic or endothermic. If δQ^\downarrow is the amount of heat received by the system under investigation during the reaction



then $\delta Q^\downarrow < 0$ for exothermic reactions and $\delta Q^\downarrow > 0$ for endothermic reactions.

Let us consider the following situation: A piece of metal is surrounded by H_2 -gas at constant pressure $p_{H_2} = p_0$ and at constant temperature $T=T_0$. We assume that δN_H hydrogen atoms are transferred from the gas to the metal. The heat δQ^\downarrow absorbed by the whole system in a reversible process at constant $T=T_0$ and $p=p_0$ is



(III.3)

$$\delta Q^\downarrow = T_0 \delta S = \delta H$$

since

$$H = U + pV \quad (\text{III.4})$$

The heat of formation is thus equal to the change in enthalpy δH . To calculate it we use the fact that at equilibrium the surrounding hydrogen is in thermodynamic equilibrium with *one* metal hydride phase MH_x and consequently

$$\frac{1}{2} \mu_{H_2}(p, T) = \mu_H(p, T, c_H) \quad (\text{III.5})$$

where μ_{H_2} is the chemical potential of pure molecular hydrogen (which, at room temperature, is in the gaseous state at pressures lower than 53 kbar) and μ_H is the chemical potential of atomic hydrogen in solution in the metal. By differentiating Eq.III.5 with respect to $1/T$ at constant concentration $c_H \equiv [H]/[M]$ we obtain

$$\begin{aligned} & \frac{1}{2} \frac{\partial(\mu_{H_2}/T)}{\partial(1/T)} \Big|_p + \frac{1}{2} \frac{\partial(\mu_{H_2}/T)}{\partial p} \Big|_T \frac{\partial p}{\partial(1/T)} \Big|_{c_H} \\ &= \frac{\partial(\mu_H/T)}{\partial(1/T)} \Big|_{p,c_H} + \frac{\partial(\mu_H/T)}{\partial p} \Big|_T \frac{\partial p}{\partial(1/T)} \Big|_{c_H} \end{aligned} \quad (\text{III.6})$$

Using the general relations

$$\frac{\partial \mu}{\partial p} \Big|_{n,T} = \frac{\partial^2 G}{\partial p \partial n} \Big|_T = \frac{\partial \mathcal{V}}{\partial n} \Big|_{p,T} \equiv \bar{V} \quad (\text{III.7})$$

$$\frac{\partial(\mu/T)}{\partial(1/T)} \Big|_{p,n} = \frac{\partial H}{\partial n} \Big|_{p,T} \equiv \bar{H} \quad (\text{III.8})$$

we can rewrite Eq.III.6 in the following form

$$\Delta \bar{H} = \bar{H}_H - \frac{1}{2} \bar{H}_{H_2} = \left(\bar{V}_H - \frac{1}{2} \bar{V}_{H_2} \right) \frac{\partial p}{\partial \ln T} \Big|_{c_H} \quad (\text{III.9})$$

G is the Gibbs free energy of the total system, n the number of moles, \bar{H} is the **partial molar enthalpy** and \bar{V} the **partial molar volume**. The quantity $\Delta H \equiv \bar{H}_H - \frac{1}{2} \bar{H}_{H_2}$ is the **partial molar heat of solution of hydrogen in a metal** per gram-atom of hydrogen.

There is some experimental evidence that \bar{V}_H , the partial molar volume of hydrogen in a metal, is independent of pressure and temperature. It is therefore possible to determine $\Delta \bar{H}$ from a plot of p versus $\ln T$ once the pressure and temperature dependence of the enthalpy H_{H_2} and V_{H_2} of pure hydrogen are known. Values of the thermodynamic properties in the temperature range 100 K to 1000 K at pressures up to 1 Mbar given by Hemmes et al.¹⁶. Values for V_H are given in the review articles of Peisl¹⁷ and Westlake¹⁸. Bouten and Miedema¹⁹ and Griessen and Feenstra²⁰ apply their semi-empirical models to the calculation of the partial molar volume.

At low pressures ($p < 100$ bar) the partial molar volume of hydrogen gas is much larger than \bar{V}_H (which is typically $1.7 \text{ cm}^3/\text{mole H}$) and H_2 behaves approximately as an ideal gas, i.e. $pV_{H_2} \cong RT$. Equation III.9 then simplifies to

$$\bar{H}_H - \frac{1}{2} \bar{H}_{H_2}^0 \cong \frac{R}{2} \frac{\partial \ln p}{\partial(1/T)} \Big|_{c_H} \quad (\text{III.10})$$

Since H_{H_2} is nearly independent of pressure in this regime, we have replaced H_{H_2} by its value at the standard pressure of one atmosphere.

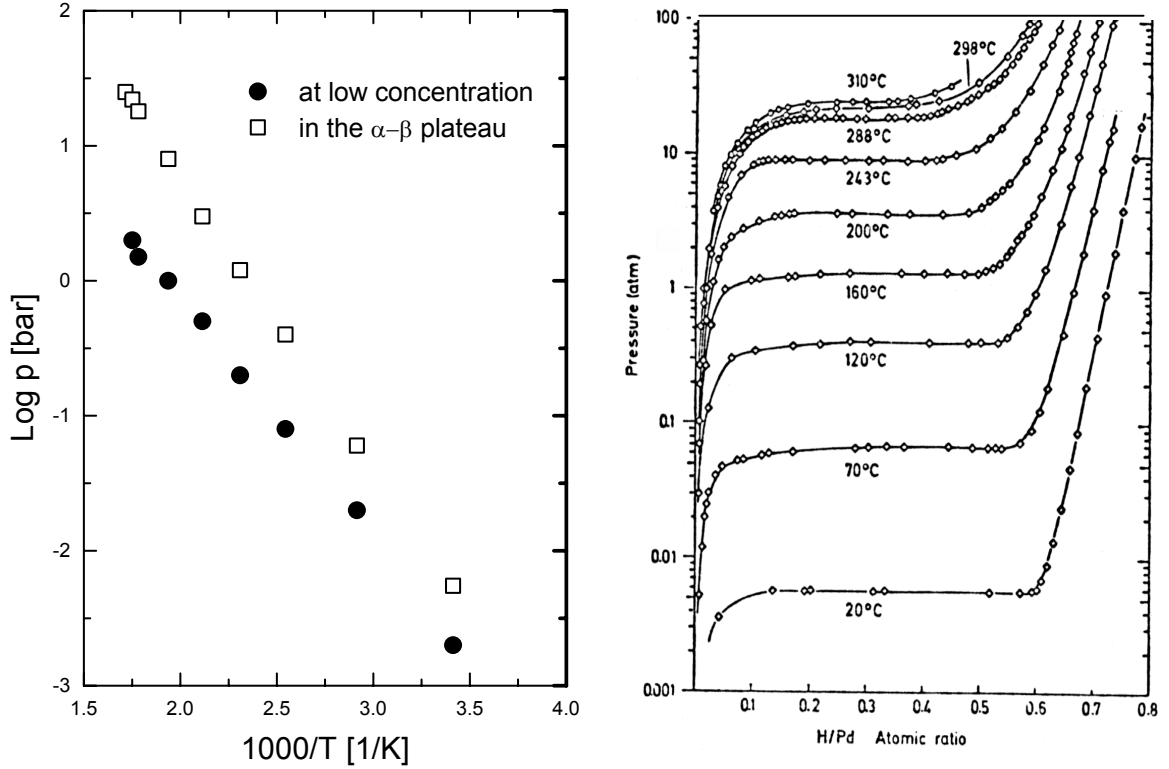


Fig. III.16: Van t'Hoff plots constructed from the isotherms in the right panel. The slope of the lines give the enthalpy of formation. The black dots are for a low hydrogen concentration $H/Pd=0.01$, while the red squares correspond to the plateau region.

As indicated in Fig. III.15 and in Table III.1 the absorption of hydrogen in a metal can be exothermic or endothermic. For the early transition-metal hydrides, for example one finds large negative values for ΔH (exothermic). For the late transition metals as well as for the majority of the simple metals ΔH is positive (endothermic). In contrast to exothermic systems, the metals with $\Delta H > 0$ absorb only small quantities of hydrogen at moderate pressures. For such systems one often carries out experiments at constant pressure and determines the temperature dependence of the solubility of hydrogen in a given metal. From these data one can derive the partial heat of solution in the following way.

At constant pressure Eq.III.5 leads to

$$-\left. \frac{\partial(\mu_H/T)}{\partial c_H} \right|_{p,T} - \left. \frac{\partial c_H}{\partial(1/T)} \right|_p = \bar{H}_H - \frac{1}{2} \bar{H}_{H_2} \quad (\text{III.11})$$

The first derivative in Eq.III.11 can be written as

$$\frac{1}{T} \left. \frac{\partial \bar{H}_H}{\partial c_H} \right|_{p,T} - \left. \frac{\partial \bar{S}_H}{\partial c_H} \right|_{p,T} \quad (\text{III.12})$$

In the limit of infinite dilution $\left(\frac{\partial \bar{H}_H}{\partial c_H}\right)_{p,T}$ tends towards a constant. The entropy \bar{S}_H , however, diverges because of the contribution $-R \ln[c_H/(1-c_H)]$ of the mixing entropy term (this expression will be derived in the chapter on the lattice gas; see Eq.III.92). We then have for $c_H \rightarrow 0$

$$\left.\frac{\partial(\mu_H/T)}{\partial c_H}\right|_{p,T} \rightarrow \frac{R}{c_H} \quad (\text{III.13})$$

$$\Delta \bar{H} = -R \left.\frac{\partial \ln c_H}{\partial (1/T)}\right|_p \quad (\text{III.14})$$

The partial molar heat of solution $\Delta \bar{H}$ may thus be obtained from a $\ln c_H$ or a $\ln x$ versus inverse temperature plot.

Until now we have only considered the situation of a homogeneously hydrogenated metal in equilibrium with pure hydrogen gas. However, many metal-hydrogen systems exhibit miscibility gaps for which **two** metal-hydride phases, say α and β , coexist and are in equilibrium with the surrounding hydrogen gas. Below a critical temperature the pressure-composition isotherms have a plateau for hydrogen concentrations between c_α and c_β . The conditions for thermodynamic equilibrium between the α and β phases and H_2 are

$$\mu_H^\alpha(p, T, c_\alpha) = \mu_H^\beta(p, T, c_\beta) = \frac{1}{2} \mu_{H_2}(p, T) \quad (\text{III.15})$$

and

$$\mu_M^\alpha(p, T, c_\alpha) = \mu_M^\beta(p, T, c_\beta) \quad (\text{III.16})$$

The atomic fractions c_α and c_β are independent variables.

The conditions for thermodynamical equilibrium between phases given above are derived as follows. We assume that we have the following three different phases in contact with each other,

- Hydrogen H_2 gas at pressure p
- a low concentration (c_α) metal-hydrogen phase (α)
- a high-concentration (c_β) metal-hydrogen phase (β) with $c_\alpha < c_\beta$

as shown in Fig. III.17.

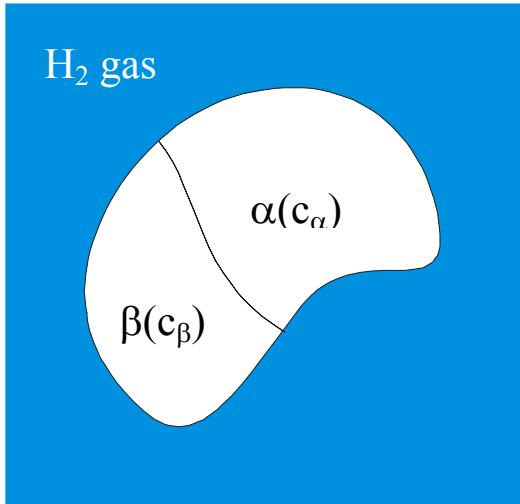


Fig. III.17: A two-phase metal-hydride system in a hydrogen gas atmosphere.

In a “chemical” language we would write the following reactions



These reactions can be written in the general form

$$\sum_{i=1}^n m_i A_i = 0 \quad (n = \text{number of substances})
 \tag{ III.18}$$

At equilibrium we know that the Gibbs free energy $G=U-TS+pV$ has a minimum, for given p and T . The only possible reactions are those for which $\delta G=0$, thus

$$\delta G = \frac{\partial G}{\partial p} \delta p + \frac{\partial G}{\partial T} \delta T + \sum_i \frac{\partial G}{\partial N_i} \delta N_i = 0
 \tag{ III.19}$$

At p and T constant

$$\delta G = \sum_i \mu_i \delta N_i = 0
 \tag{ III.20}$$

where we have used the definition of the chemical potential

$$\mu_i = \left. \frac{\partial G}{\partial N_i} \right|_{p, T, N_{j \neq i}}
 \tag{ III.21}$$

Dividing Eq.III.20 by, say δN_1 , gives

$$\mu_1 + \sum_{j=2} \mu_j \frac{\delta N_j}{\delta N_1} = 0 \quad (\text{III.22})$$

Equation III.18 implies, however, that

$$\frac{\delta N_j}{\delta N_1} = -\frac{m_j}{m_1} \quad (\text{III.23})$$

and thus, the condition for equilibrium is

$$\sum_{i=1}^n \mu_i m_i = 0 \quad (\text{III.24})$$

For the three reactions given in Eq.III.17 we have thus

$$\begin{aligned} \frac{1}{2} \mu_{H_2}(p, T) &= \mu_H(c_\alpha, T) \equiv \mu_H^\alpha && \text{for hydrogen} \\ \frac{1}{2} \mu_{H_2}(p, T) &= \mu_H(c_\beta, T) \equiv \mu_H^\beta && \text{for hydrogen} \\ \mu_M(c_\alpha, T) &= \mu_M(c_\beta, T) \Rightarrow \mu_M^\alpha = \mu_M^\beta && \text{for the metal} \end{aligned} \quad (\text{III.25})$$

The corresponding Gibbs-Duhem equations are, at constant p and T,

$$c_\alpha \frac{\partial \mu_H^\alpha}{\partial c_\alpha} + \frac{\partial \mu_M^\alpha}{\partial c_\alpha} = 0 \quad (\text{III.26})$$

and

$$c_\beta \frac{\partial \mu_H^\beta}{\partial c_\beta} + \frac{\partial \mu_M^\beta}{\partial c_\beta} = 0 \quad (\text{III.27})$$

Consider now the following derivative taken along the coexistence line defined by the equilibrium conditions (Eqs.III.15 and 16) given above,

$$\frac{d(\mu_j^v/T)}{d(1/T)} = \frac{\partial(\mu_j^v/T)}{\partial(1/T)} + \frac{\partial(\mu_j^v/T)}{\partial p} \frac{\partial p}{\partial(1/T)} + \frac{\partial(\mu_j^v/T)}{\partial c_v} \frac{\partial c_v}{\partial(1/T)} \quad (\text{III.28})$$

Using the standard relations (Eqs.III.7 and 8) we obtain

$$\frac{d(\mu_j^v/T)}{d(1/T)} = \bar{H}_j^v + \frac{\bar{V}_j^v}{T} \frac{\partial p}{\partial(1/T)} + \frac{\partial(\mu_j^v/T)}{\partial c_v} \frac{\partial c_v}{\partial(1/T)} \quad (\text{III.29})$$

where $\nu = \alpha$ or β and $j = H$ or M .

Along the coexistence line we have, as a direct consequence of Eqs.III.15 and 16

$$\frac{d(\mu_H^\alpha/T)}{d(1/T)} = \frac{d(\mu_H^\beta/T)}{d(1/T)} = \frac{1}{2} \frac{d(\mu_{H_2}/T)}{d(1/T)} \quad (\text{III.30})$$

and

$$\frac{d(\mu_M^\alpha/T)}{d(1/T)} = \frac{d(\mu_M^\beta/T)}{d(1/T)} \quad (\text{III.31})$$

Multiplying Eq.III.29 for $\nu = \alpha$ and $j = H$ by c_α and adding it to Eq.III.29 for $\nu = \alpha$ and $j = M$ we obtain

$$c_\alpha \frac{d(\mu_H^\alpha/T)}{d(1/T)} + \frac{d(\mu_M^\alpha/T)}{d(1/T)} = H_\alpha + \frac{V_\alpha}{T} \frac{dp}{d(1/T)} \quad (\text{III.32})$$

with

$$H_\alpha \equiv c_\alpha \bar{H}_H^\alpha + \bar{H}_M^\alpha \quad (\text{III.33})$$

and

$$V_\alpha \equiv c_\alpha \bar{V}_H^\alpha + \bar{V}_M^\alpha \quad (\text{III.34})$$

For the β -phase we have similarly

$$c_\beta \frac{d(\mu_H^\beta/T)}{d(1/T)} + \frac{d(\mu_M^\beta/T)}{d(1/T)} = H_\beta + \frac{V_\beta}{T} \frac{dp}{d(1/T)} \quad (\text{III.35})$$

Subtraction of Eq.III.32 from Eq.III.35 leads, in combination with Eq.III.30 to

$$\frac{dp}{T d(1/T)} = \frac{H_\beta - H_\alpha - \frac{1}{2}(c_\beta - c_\alpha) \bar{H}_{H_2}}{\frac{1}{2}(c_\beta - c_\alpha) \bar{V}_{H_2} - (V_\beta - V_\alpha)} \quad (\text{III.36})$$

This is a general expression which is also valid under high pressure conditions. It can be simplified by using the fact that V_H^ν depends only weakly on the hydrogen concentrations and that $V_M^\beta \cong V_M^\alpha$. We then obtain

$$\Delta H_{\alpha \rightarrow \beta} \cong \left(\bar{V}_H - \frac{1}{2} \bar{V}_{H_2} \right) \frac{dp}{d \ln T} \quad (\text{III.37})$$

where $\Delta H_{\alpha \rightarrow \beta}$ is the enthalpy of formation (expressed per mole H) of the hydride $MH_{x\beta}$ from the hydrogen saturated metal solid solution of composition $MH_{x\alpha}$, i.e.

$$\Delta H_{\alpha \rightarrow \beta} = \frac{H_\beta - H_\alpha}{c_\beta - c_\alpha} - \frac{1}{2} \bar{H}_{H_2} \quad (\text{III.38})$$

or equivalently $\Delta H_{\alpha \rightarrow \beta}$ is the heat of reaction of the process



As for the case of a single hydride phase Eq.III.37 leads to

$$\Delta H_{\alpha \rightarrow \beta} \cong \frac{R}{2} \frac{\partial \ln p}{\partial (1/T)} \quad (\text{III.40})$$

A Van t'Hoff plot constructed from the plateaux in the isotherms in the right panel of Fig. III.16. is slightly steeper than at infinite dilution. In other words the partial molar enthalpy of formation is concentration dependent²¹.

The general thermodynamic relations derived here make it possible to determine thermodynamic quantities from experimental values. In order to develop a certain “feeling” for these quantities it is, however, necessary to use a model. In the next sections we consider the so-called **lattice-gas model**.

III.3 MEAN-FIELD THEORY OF THE LATTICE-GAS

The thermodynamical relations derived so far are general but do not provide the reader with much intuition. For this we consider one of the simplest models for an interstitial alloy consisting of a rigid lattice of metal atoms and mobile interstitial hydrogen atoms.

From the similarity between M-H phase diagrams and solid-liquid-gas phase diagrams one is tempted to conclude that H in a metal behaves almost like a gas at low concentrations and exhibits condensation phenomena analogous to a gas-liquid system. However, because of the presence of the host metal lattice one cannot identify H in M with a free gas of H atoms (note

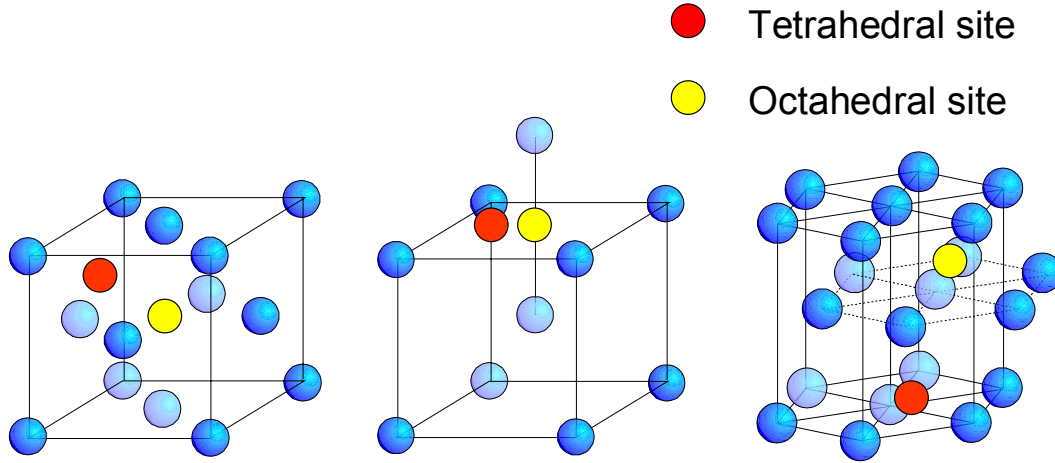


Fig. III.18: Transition metal hydrides are a realisation of the lattice-gas model in statistical physics since it occupies interstitial sites in the host metallic lattice. From left to right we show an octahedral and an tetrahedral interstitial site of the fcc, bcc and hcp lattice.

that a H_2 molecule are probably too large to be accommodated at interstitial sites in a metal). In what follows we shall postulate that H in metals can be described by means of the so-called **lattice gas** model. This model is precisely defined by Lee and Yang²² as follows:

A lattice gas is a monatomic gas with the interaction

$$U = \sum_{i,j} U(|\mathbf{R}_i - \mathbf{R}_j|) \quad (\text{III.41})$$

where \mathbf{R}_i indicates the position of the i -th atom and

- a) the atoms have a finite impenetrable core of diameter a , so that $U(r) = \infty$ for $r < a$
- b) the interaction has a finite range, so that $U(r) = 0$ for $r > b$
- c) $U(r)$ is nowhere $-\infty$

For our problem of hydrogen in a metal this means that two hydrogen atoms cannot occupy the same interstitial site and that there is some sort of interaction between two H dissolved in a metal. Without going into detail about the nature of this interaction, we shall assume, following Lacher's early treatment²³, that the energy of hydrogen atoms dissolved in a metal is given by the following expression

$$E = N_H \epsilon_o + N_{HH} \epsilon \quad (\text{III.42})$$

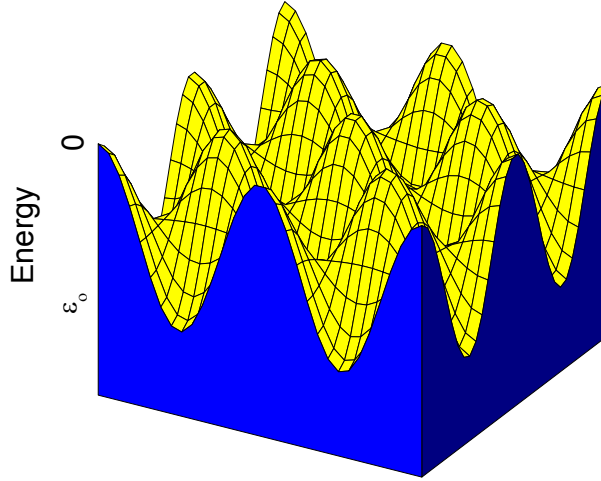


Fig. III.19 :Potential seen by one H atom in a metal. The minima correspond to interstitial sites.

where N_{HH} is the number of nearest neighbour H-pairs and ϵ is the H-H pair interaction. We take the zero of energy at the energy of a single H-atom outside the metal.

If N is the total number of sites then $N_H < N$. To determine the thermodynamical properties of the metal-hydrogen system, let us calculate the free energy $F=U-TS$ by means of the relation

$$F = -kT \ln \sum \exp \left[-\frac{N_H \epsilon_o + N_{HH} \epsilon}{kT} \right] \quad (\text{III.43})$$

where the sum (the partition function) is taken over all configurations of N_H atoms distributed over N sites. To evaluate F we need thus to calculate the number N_{HH} of H-H pairs for each distribution of the N_H atoms. This problem is completely equivalent (formally) to the **Ising model** and has not been solved analytically yet for a three dimensional gas (system). This means that we have to look for an appropriate approximation. The simplest one was formulated by Bragg and William²⁴ and assumes that there is no short range order around hydrogen atoms. This is of course only true in the limit of weak interaction between two H atoms. The use of the Bragg-William approximation leads to

$$N_{HH} = N_H n \frac{N_H}{N} \frac{1}{2} \quad (\text{III.44})$$

with n , the number of nearest neighbours interstitial sites (for example, $n=12$ for octahedral sites in a FCC lattice), and $\frac{N_H}{N}$ the probability of finding a nearest neighbour around a given H. The factor $1/2$ avoids counting the H-H pairs twice. We have thus

$$E = \epsilon_o N_H + \frac{\epsilon}{2} n \frac{N_H^2}{N} \quad (\text{III.45})$$

The energy E of a configuration depends thus only on N_H , which is of course the same for all pairs. This implies that

$$F = -kT \ln \left[\frac{N!}{N_H!(N - N_H)!} e^{-\left(\varepsilon_o N_H + \frac{\varepsilon n N_H^2}{2N} \right) / kT} \right]$$

$$= -kT \left[\ln N! - \ln N_H! - \ln(N - N_H)! - (N_H \varepsilon_o + \varepsilon \frac{n N_H^2}{2N}) / kT \right] \quad (\text{III.46})$$

Using Stirling's formula

$$\ln N! \cong N \ln N - N \quad (\text{III.47})$$

we obtain

$$F = -kT \left[N \ln N - N_H \ln N_H - (N - N_H) \ln(N - N_H) - N \left(\frac{N_H}{N} \varepsilon_o + \varepsilon \frac{n}{2} \left(\frac{N_H}{N} \right)^2 \right) / kT \right] \quad (\text{III.48})$$

Introducing the concentration c_H

$$c_H = \frac{N_H}{N} \quad (\text{III.49})$$

we have

$$F_H = kTN \left[c_H \ln c_H + (1 - c_H) \ln(1 - c_H) \right] + N \left[\varepsilon_o c_H + \varepsilon \frac{n}{2} c_H^2 \right] \quad (\text{III.50})$$

Note that c_H is not necessarily equal to x in a hydride MH_x as for certain structures N , the number of interstitial sites of a certain type may be different from the number of atoms. There are, for example, two tetrahedral sites per metal atom in a FCC structure. This is the case for YH_2 which crystallises in the so-called calcium fluorite structure.

The chemical potential μ_H of hydrogen in a metal is

$$\mu_H(c_H, T) = \left. \frac{\partial F}{\partial N_H} \right|_{T,V} = \frac{1}{N} \left. \frac{\partial F}{\partial c_H} \right|_{T,V} \quad (\text{III.51})$$

$$\mu_H = kT \ln \frac{c_H}{1-c_H} + \varepsilon_o + \varepsilon n c_H \quad (\text{III.52})$$

We show now that it is possible to determine μ_H by measuring solubility isotherms (see Fig. III.2, Fig.III.4, and Fig. III.6). For this type of measurements the M-H sample is surrounded by H_2 gas in equilibrium with a certain H/M value. At thermodynamical equilibrium the chemical potentials of the two phases are equal and we obtain from Eqs. III.52 and II.78

$$\frac{1}{2} \left(\varepsilon_b + kT \ln \frac{p}{p_0(T)} \right) = kT \ln \frac{c_H}{1-c_H} + \varepsilon_o + \varepsilon n c_H \quad (\text{III.53})$$

This equation describes the solubility isotherms in the one phase region. In the limit of small hydrogen gas pressure we have simply

$$\begin{aligned} \frac{1}{2} kT \ln \frac{p}{p_0(T)} &\cong kT \ln c_H \\ p \rightarrow 0 \quad c_H &\rightarrow 0 \end{aligned} \quad (\text{III.54})$$

which is known as **Sievert's law**:

"The equilibrium concentration of hydrogen dissolved in a metal is proportional to the square root of the H_2 pressure".

It can be seen that Sievert's law is relatively well obeyed in Fig. III.20 (for PdH_x) and Fig.III.21 (for NbH_x).

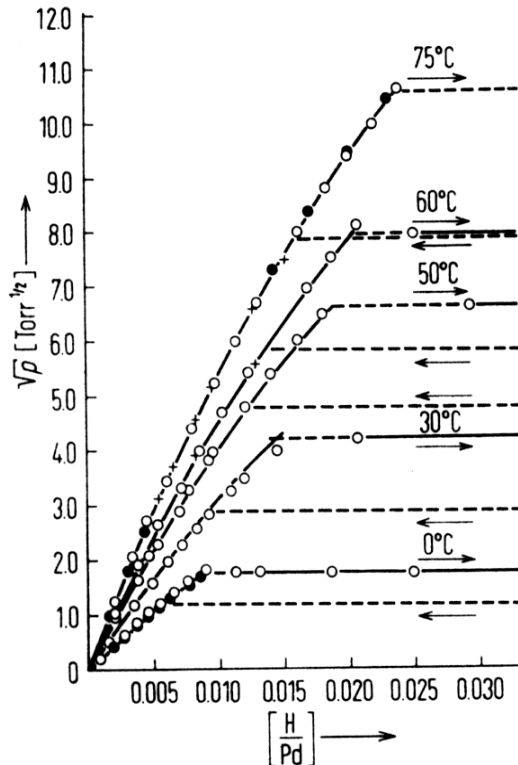


Fig. III.20: Solubility isotherms for PdH in the α -phase (see phase diagram in Fig.II.6). The kink in the curves correspond to the onset of the mixed-phase region. (Note the pressure scale, which is $p^{1/2}$). Wicke and Nernst.

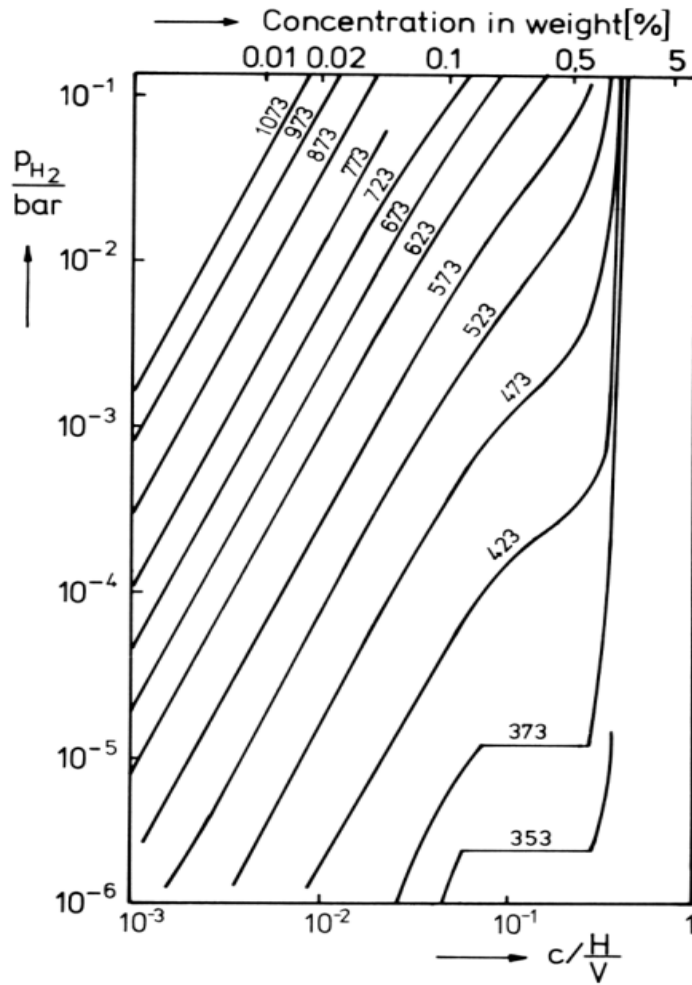


Fig.III.21: Solubility isotherms for VH_x in a double-log representation to emphasize the low hydrogen concentration regime. The temperatures are given in degrees Kelvin. The slope $d \ln c / d \ln p_{H_2}$ of the low concentration straight lines is equal to $1/2$ as expected from Sievert's law. [Schober et al.]

Equation III.53 may, however, be unphysical at low temperatures (by low we mean in fact $T < T_c$ where T_c is the critical point of the MH_x system under consideration). This can be seen as follows. From Eq.III.53 we have

$$\frac{1}{2} \left(\varepsilon_b - \varepsilon n + kT \ln \frac{p}{p_0(T)} - 2\varepsilon_0 \right) = f(c_H) \quad (\text{III.55})$$

where

$$f(c_H) = kT \ln \frac{c_H}{1-c_H} + \varepsilon n \left(c_H - \frac{1}{2} \right) \quad (\text{III.56})$$

The function $y=f(c_H)$ is antisymmetric with respect to the point $c_H=1/2$ and $y=0$. The solubility isotherms can therefore have the following shape (see Fig. III.22).

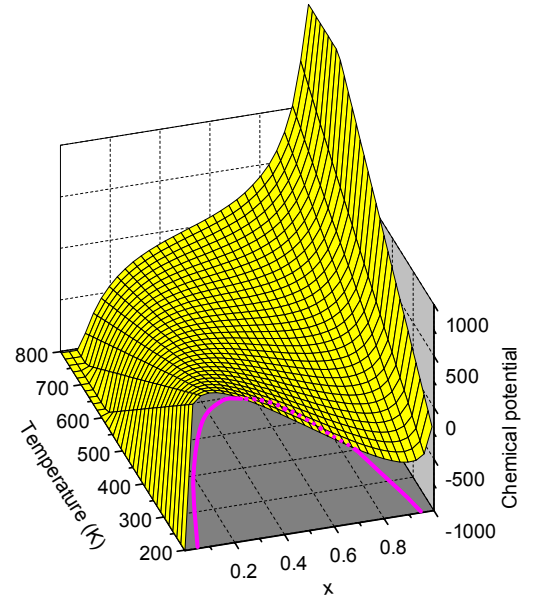
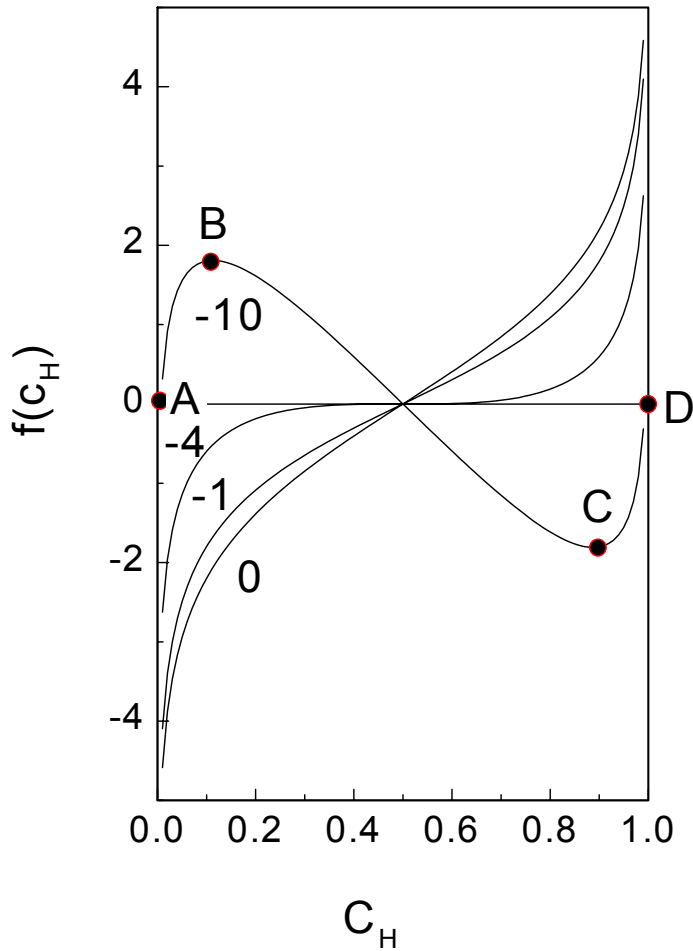


Fig. III.22: The function $f(c_H)$ for four values of the parameter $\epsilon n/kT$, i.e. 0, -1, -4, -10. In the right panel, a 3D representation of the chemical potential of a lattice-gas. The violet curve corresponds to the locus of the maxima and minima. We shall see later that this defines the so-called spinodal curve.

We shall see that a necessary condition for thermodynamic equilibrium is that

$$\left. \frac{\partial \mu_H}{\partial c_H} \right|_{p,T} \geq 0 \quad (\text{III.57})$$

As

$$\left. \frac{\partial \mu_H}{\partial c_H} \right|_{p,T} = \frac{\partial f}{\partial c_H} \quad (\text{III.58})$$

the states between B and C are unphysical. In terms of free energy, it means that F_H has a shape as indicated in Fig. III.23.

This figure represents the free energy of a MH_x system in a single phase. We shall show now, for $c_\alpha \leq c_H \leq c_{\alpha'}$, where the concentrations c_α and $c_{\alpha'}$ are determined by the so-called “common

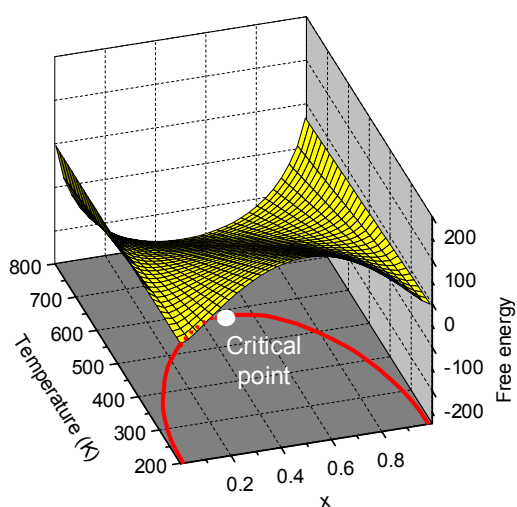
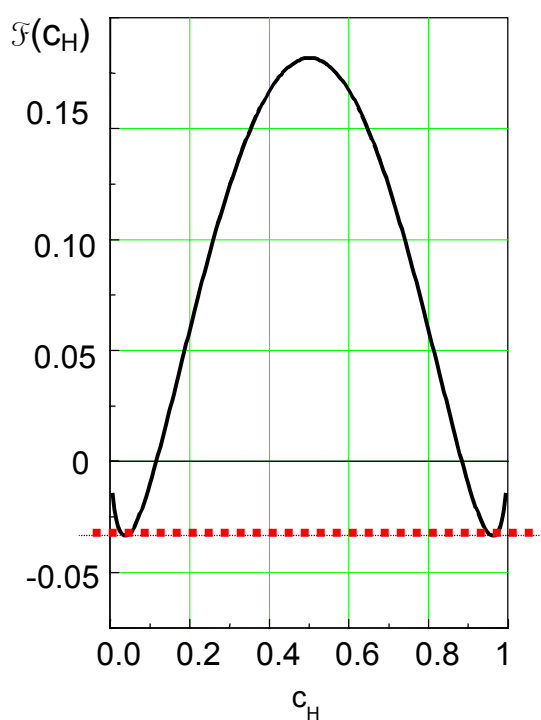
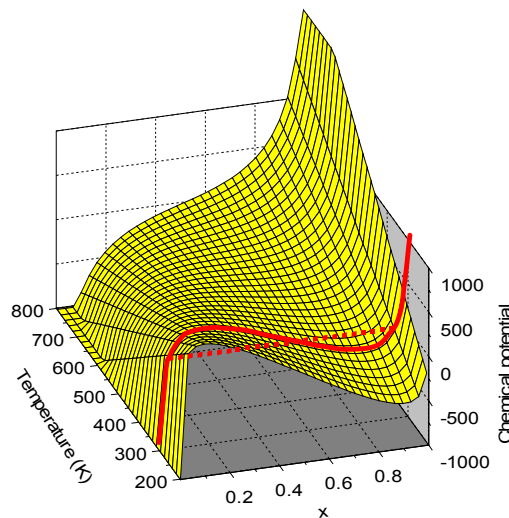
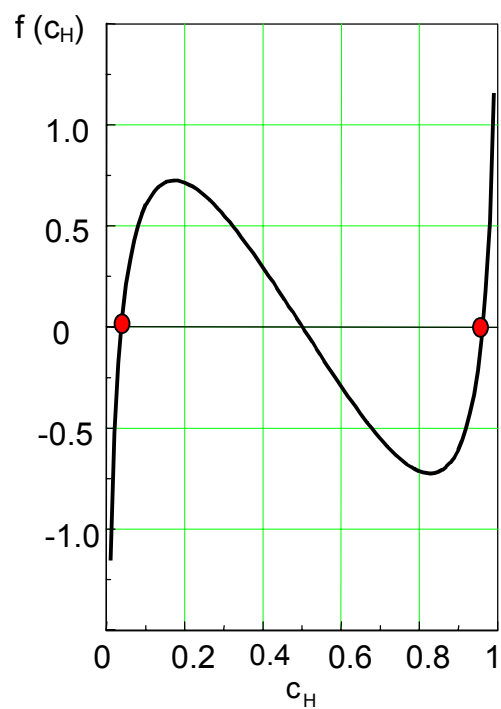


Fig. III.23: The function $f(c_H)$ and its integral $\mathcal{F}(c_H)$ for $\epsilon n/kT=7$. The dashed red line corresponds to the common tangent construction implied by Eq.III.66. In the right panels, we show 3D representations of the chemical potential and the free energy and the Maxwell construction to determine the coexistence curve corresponding to the red curve in the lower-right panel.

tangent” construction, that the free energy of the system can be minimized by assuming a mixed-phase such that

$$c_\alpha x_\alpha + c_{\alpha'} x_{\alpha'} = c_H \quad (\text{III.59})$$

where x_α is the fraction of the sample in the α -phase with $N_H^\alpha / N^\alpha = c_\alpha$ and

$$x_\alpha + x_{\alpha'} = 1 \quad (\text{III.60})$$

From Eq.III.50 for F follows for the Gibbs free energy (neglecting pressure effects) that

$$\begin{aligned} G_{tot} = G_{H_2}(p, T) + \\ x_\alpha \left\{ kTN [c_\alpha \ln c_\alpha + (1 - c_\alpha) \ln(1 - c_\alpha)] + N \left[\varepsilon_0 c_\alpha + \frac{\varepsilon n}{2} c_\alpha^2 \right] \right\} + \\ x_{\alpha'} \left\{ kTN [c_{\alpha'} \ln c_{\alpha'} + (1 - c_{\alpha'}) \ln(1 - c_{\alpha'})] + N \left[\varepsilon_0 c_{\alpha'} + \frac{\varepsilon n}{2} c_{\alpha'}^2 \right] \right\} \end{aligned} \quad (\text{III.61})$$

For a minimum of G_{tot} at given p and T we need

$$\left. \frac{\partial G}{\partial x_\alpha} \right|_{c_H, c_\alpha} = 0 \quad \text{and} \quad \left. \frac{\partial G}{\partial c_\alpha} \right|_{c_H, x_\alpha} = 0 \quad (\text{III.62})$$

if x_α and c_α are chosen as independent variables.

$$\begin{aligned} \frac{1}{N} \left. \frac{\partial G}{\partial c_\alpha} \right|_{c_H, x_\alpha} = x_\alpha \left[kT \ln \frac{c_\alpha}{1 - c_\alpha} + \varepsilon_0 + \varepsilon n c_\alpha \right] \\ + x_{\alpha'} \left[kT \ln \frac{c_{\alpha'}}{1 - c_{\alpha'}} + \varepsilon_0 + \varepsilon n c_{\alpha'} \right] \left. \frac{dc_{\alpha'}}{dc_\alpha} \right|_{c_H, x_\alpha} = 0 \end{aligned} \quad (\text{III.63})$$

This implies that the two expressions in the square brackets must be equal. This is nothing else than the equality of the chemical potentials $\mu_\alpha = \mu_{\alpha'}$

$$\begin{aligned}
\left. \frac{1}{N} \frac{\partial G}{\partial x_\alpha} \right|_{c_H, \varepsilon_\alpha} &= kT [c_\alpha \ln c_\alpha + (1-c_\alpha) \ln(1-c_\alpha)] \\
&+ \varepsilon_0 c_\alpha + \frac{\varepsilon}{2} n c_\alpha^2 \\
&+ \frac{dx_{\alpha'}}{dx_\alpha} \left\{ kT [c_{\alpha'} \ln c_{\alpha'} + (1-c_{\alpha'}) \ln(1-c_{\alpha'})] + \varepsilon_0 c_{\alpha'} + \frac{\varepsilon}{2} n c_{\alpha'}^2 \right\} \\
&+ x_{\alpha'} \frac{dc_{\alpha'}}{dx_\alpha} \left\{ kT \ln \frac{c_{\alpha'}}{1-c_{\alpha'}} + \varepsilon_0 + \varepsilon n c_{\alpha'} \right\}
\end{aligned} \tag{III.64}$$

$$\text{with } \frac{dx_{\alpha'}}{dx_\alpha} = -1 \text{ and } \frac{dc_{\alpha'}}{dx_\alpha} = \frac{c_{\alpha'} - c_\alpha}{1 - x_\alpha}$$

Thus $\left. \frac{\partial G}{\partial x_\alpha} \right|_{c_H, \varepsilon_\alpha} = 0$ implies that,

$$\begin{aligned}
&kT [c_\alpha \ln c_\alpha + (1-c_\alpha) \ln(1-c_\alpha)] + \varepsilon_0 c_\alpha + \frac{\varepsilon}{2} n c_\alpha^2 \\
&- kT \left([c_{\alpha'} \ln c_{\alpha'} + (1-c_{\alpha'}) \ln(1-c_{\alpha'})] + \varepsilon_0 c_{\alpha'} + \frac{\varepsilon}{2} n c_{\alpha'}^2 \right) \\
&+ (c_{\alpha'} - c_\alpha) \left[kT \ln \frac{c_{\alpha'}}{1-c_{\alpha'}} + \varepsilon_0 + \varepsilon n c_{\alpha'} \right] = 0
\end{aligned} \tag{III.65}$$

In a more compact form

$$G(c_\alpha) - G(c_{\alpha'}) + (c_{\alpha'} - c_\alpha) \frac{\partial G}{\partial c_{\alpha'}} = 0 \tag{III.66}$$

which means that c_α and $c_{\alpha'}$ are given by the common tangent construction indicated in Fig. III.23 as $\partial G / \partial c_{\alpha'} = \partial G / \partial c_\alpha$ from Eq.III.64. To determine c_α and $c_{\alpha'}$ analytically let us express Eq.III.66 in terms of the function f defined in Eq.III.56 and its integral \mathcal{F} . We obtain,

$$\mathcal{F}(c_\alpha) - \mathcal{F}(c_{\alpha'}) + (c_{\alpha'} - c_\alpha) f = 0 \tag{III.67}$$

\mathcal{F} is a symmetric function with respect to a vertical axis at $c=1/2$ and the solution of Eq.III.66 is given by

$$f(c_\alpha) = 0 \tag{III.68}$$

which is equivalent to $\mathcal{F}(c_\alpha) = \mathcal{F}(c_{\alpha'})$. Thus if $c_\alpha = 1/2 - \delta$ then $c_{\alpha'} = 1/2 + \delta$

The two coexisting phases have concentrations c_α and c_α' given by

$$kT \ln \frac{c_i}{1-c_i} + \varepsilon n (c_i - \frac{1}{2}) = 0 \quad (\text{III.69})$$

and the corresponding pressure, the dissociation pressure p_{dis} is given by Eq.III.55

$$kT \ln \frac{p_{dis}}{p_0(T)} = 2\varepsilon_0 + \varepsilon n - \varepsilon_b \quad (\text{III.70})$$

We shall now discuss implications of Eq.III.53, Eq.III.69 and III.70.

III.3.1 PLATEAU DISSOCIATION PRESSURES

From Eq.III.70 follows that

$$\ln p_{dis} = \ln p_0(T) + \frac{2\varepsilon_0 + \varepsilon n - \varepsilon_b}{kT} \quad (\text{III.71})$$

However, in the temperature range 20 °C - 300 °C for which $\ln p_0 \sim \text{constant}$, this equations reduces to

$$\ln p_{dis}(T) \cong \text{const.} + \frac{2\varepsilon_0 + \varepsilon n - \varepsilon_b}{kT} \quad (\text{III.72})$$

in very good agreement with the results shown in Fig. III.16 for PdH_x. The slope of the $\ln p$ vs. $1/T$ curves shown for example in Fig. III.16 gives $(2\varepsilon_0 + \varepsilon n - \varepsilon_b)/k$. The binding energy ε_b of two H atoms in a H₂ molecule is $\varepsilon_b = -4.46$ eV. Thus

$$\begin{aligned} 2\varepsilon_0 + \varepsilon n &= \text{slope} \cdot k - 4.46 \text{ eV} \\ \text{with } k &= 8.62 \cdot 10^{-5} \text{ eV K}^{-1} \end{aligned} \quad (\text{III.73})$$

For PdH_x one finds $2\varepsilon_0 + \varepsilon n \cong -4.9$ eV. For most metal-hydrides, $2\varepsilon_0 + \varepsilon n$ is lower than -5 eV and can reach approximately -6.4 eV for LaH_x. Van t'Hoff plots for representative metal-hydride systems are indicated in Fig. III.24.

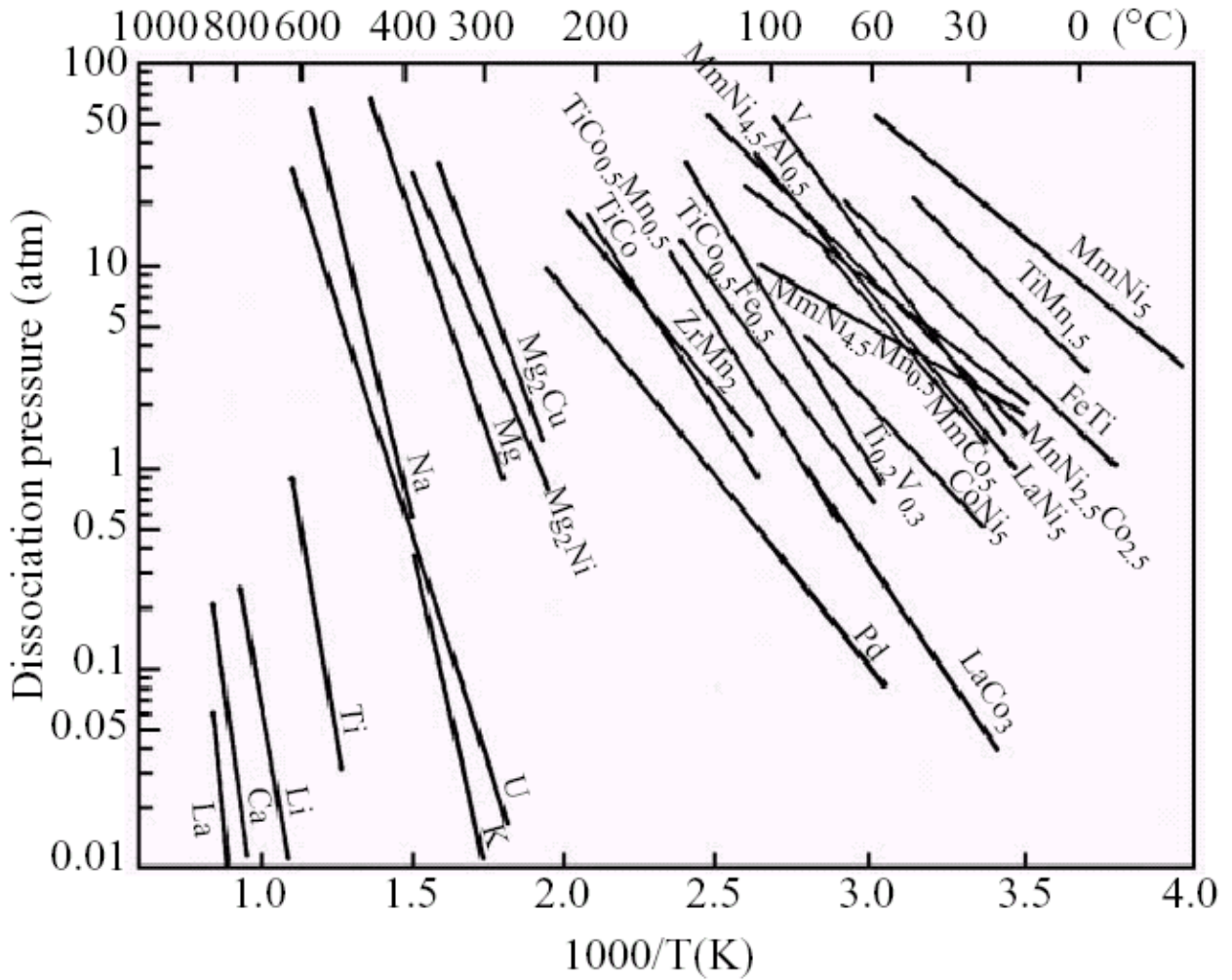


Fig. III.24: Plateau dissociation pressure for various hydrides²⁵. Note that these curves should end at the critical point of the indicated systems as Eq. II.51 is only valid for $T < T_c$, i.e. when two phases coexist.

III.3.2 DETERMINATION OF THE H-H INTERACTION PARAMETER

The values of ε_0 and ε_n may be determined separately by plotting isotherms for one-phase systems. From Eq.III.53 we have then

$$\ln \left[\frac{p}{p_0(T)} \left(\frac{1 - c_H}{c_H} \right)^2 \right] = \frac{2\varepsilon_0 - \varepsilon_b + 2\varepsilon_n c_H}{kT} \quad (\text{III.74})$$

A typical example is given in Fig. III.25 for the α -phase of PdH_x .

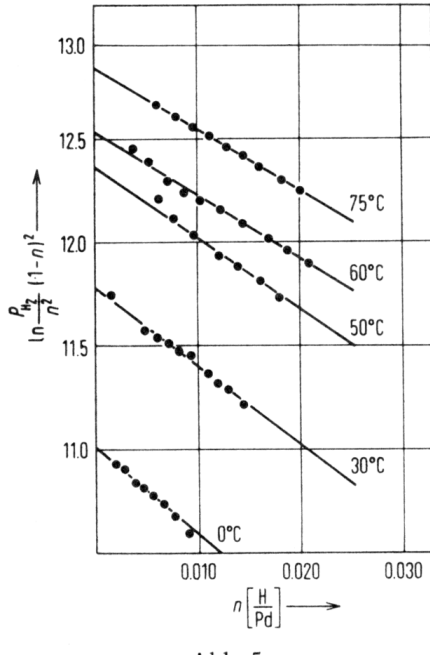


Fig. III.25: Solubility isotherms for α -PdH_x plotted according to Eq. II.55. At 30°C $\epsilon n = -0.5$ eV and $\epsilon_0 = -2.3$ eV. [see Wicke and Nernst²⁶]. Similar values have been found by Veleckis (1960) $\epsilon n = -0.35$ eV and $\epsilon_0 = -2.58$ eV for NbH_x.

III.3.3 COEXISTENCE CURVE

The coexistence curve, which defines the portion of the T-c_H diagram where two phases coexist is given by Eq. III.69. It is a curve which is symmetric relative to c_H=1/2 with a maximum at T=T_c. The critical temperature T_c is obtained from the maximum of the T(c_H) function. By differentiating Eq. III.69, we obtain

$$k \frac{dT}{dc} \Big|_{T=T_c} \ln \frac{c_c}{1-c_c} + kT_c \frac{1}{c_c(1-c_c)} + \epsilon n = 0 \quad (\text{III.75})$$

Because of the symmetry of the T(c) curve, the maximum T=T_c corresponds to a critical concentration c_c=1/2. Thus

$$T_c = -\frac{\epsilon n}{4k} \quad (\text{III.76})$$

Physically, this equation means just that order (=separation into two phases) can only exist up to a certain temperature which is of the order of the H-H interaction energy. From Eq. III.76 we obtain

$$\text{PdH}_x \quad \epsilon n = -0.20 \text{ eV} \quad T_c = 566 \text{ K} \quad (\text{III.77})$$

$$\text{NbH}_x \quad \epsilon n = -0.16 \text{ eV} \quad T_c = 443 \text{ K} \quad (\text{III.78})$$

These values are significantly smaller than the values found by Wicke and Nernst and Veleckis. They are also smaller than the values derived from the fitted equation of Simons and Flanagan²⁷ who found

$$\ln p[atm.] = 13.04 - \frac{2327}{T} - \frac{11110}{T}x + 2 \ln \frac{x}{1-x} \quad (\text{III.79})$$

which is exactly of the same form as Eq.III.53. Thus,

$$\frac{2\varepsilon n}{kT} c_H = -\frac{11110}{T}x \quad (\text{III.80})$$

from which

$$\varepsilon n = -0.48 \text{ eV} \quad (\alpha - \text{phase PdH}_x, 0^\circ - 90^\circ \text{ C})$$

In an experiment de Ribaupierre and Manchester²⁸ found that between 485 K and 619 K

$$\varepsilon n = -0.28 \text{ eV} \quad (\text{III.81})$$

for α -PdH_x

One major reason for the scatter in experimental values for εn is due to the different interpretations of the quantity $c_H = N_H/N$ which enters Eq.III.53. There are essentially two points of views:

- a) One can assume that all the interstitial sites (the octahedral sites for example in Pd) may be occupied by H. Then c_H is equal to H/Pd and the theory predicts a critical concentration of 50 % H in Pd. This is in disagreement with the experimental phase diagrams (for which $c_c \sim 30\%$). One is then forced to assume that Eq.III.53 is only valid in the limit of low concentrations. This is the view adopted by Wicke and Nernst Simons and Flanagan). De Ribaupierre and Manchester^{28, 29}, assume however implicitly that Eq.III.53 is valid over a much wider range (up to 40 % H in Pd). In this interpretation it is not meaningful to use Eq.III.76 for an evaluation of εn .
- b) One can postulate that only a certain fraction of the interstitial sites are available for H. In order to reproduce the phase diagrams of Pd-H one takes then $N=0.6 N_{Pd}$ where N_{Pd} is the number of Palladium atoms. With this choice it is possible to reproduce quite accurately the measured solubility isotherms over the whole range of H/Pd as shown by Lacher) (see Fig. III.26). The value of this approach is more mathematical than physical since it predicts diverging isotherms at 0.6 in contradiction with the experiment

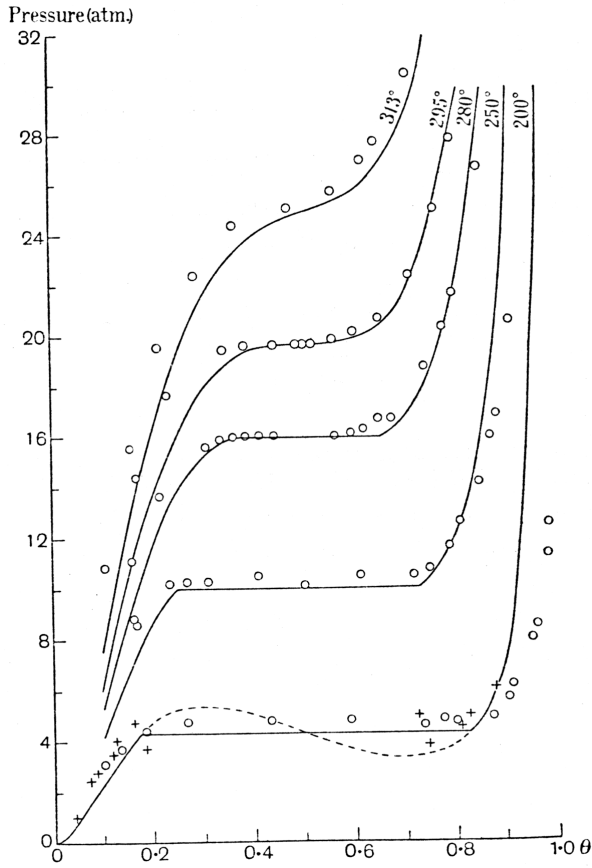


Fig. III.26: Isotherms of PdH_x compared to the predictions of the Lacher model.

As can be seen from Fig. III.26 the function fitted by Lacher

$$\ln p[\text{atm.}] = 2 \ln \frac{x}{0.59 - x} + 10.60 - \frac{2052}{T} - \frac{7700x}{T} \quad (\text{III.82})$$

with $x = \text{H/Pd}$ gives a rather good fit to the experimental data. By comparison with Eq.II.33

$$2\varepsilon n = -\frac{7700}{1.69} k \quad (\text{III.83})$$

and thus $\varepsilon n = -0.20 \text{ eV}$ in perfect agreement with Eq.III.77.

It is gratifying, to a certain extent that for both interpretations of Eq.III.53 the values for εn do not differ too much from each other. We conclude thus that the hydrogen pair interaction ε in a M-H system such as PdH_x and NbH_x is typically of the order of

$$\begin{aligned}
n=12 \xrightarrow[\text{octahedral sites}]{\text{FCC}} \varepsilon \sim -0.02 \text{ eV / pair} \quad (\text{PdH}_x) \\
n=4 \xrightarrow[\text{tetrahedral sites}]{\text{BCC}} \varepsilon \sim -0.09 \text{ eV / pair} \quad (\text{NbH}_x)
\end{aligned} \tag{III.84}$$

In the remaining part of this subsection let us come back to the shape of the coexistence curve. An approximate relation valid for low concentrations $c_H \rightarrow 0$ is readily obtained from Eq.III.69, as

$$kT \ln c_\alpha - \frac{\varepsilon n}{2} = 0 \rightarrow c_\alpha = e^{\frac{\varepsilon n}{2kT}} \tag{III.85}$$

This implies that at low temperatures the solubility of hydrogen is extremely small, if the system is in a state of thermodynamical equilibrium. Metastable states are however possible for concentrations between A and B and between C and D in Fig. III.22.

The locus of the concentrations corresponding to point B and C is called the **spinodal line** and is given by the condition

$$\frac{\partial^2 G_H}{\partial c_H^2} = 0 \tag{III.86}$$

which is equivalent to

$$\frac{\partial \mu_H}{\partial c_H} = 0 \tag{III.87}$$

From Eq.III.52 we find

$$\frac{\partial \mu_H}{\partial c_H} = kT_{sp.} \frac{1}{c_H(1-c_H)} + \varepsilon n = 0 \tag{III.88}$$

and thus $T_{sp.}$ ($=T_{\text{spinodal}}$)

$$T_{sp.} = -\frac{\varepsilon n}{k} c_H(1-c_H) \tag{III.89}$$

is a parabola with its maximum at the critical point T_c . Both the coexistence curve and the spinodal curve are shown in Fig. III.28. We shall come back to the notion of spinodal decomposition in a later Chapter.

Fig. III.27: (Three panels on the right); Chemical potential of the lattice gas as a function of temperature. The interaction term is $\epsilon_n = -0.2$ eV i.e. 2321 K. For clarity a constant equal to $\epsilon_0 - 0.2$ eV has been subtracted. The locus of the minima and maxima of an isotherm is the spinodal curve (violet curve in middle panel). The corresponding free energy is shown in the lower panel. For clarity the linear term $(\epsilon_0 + \epsilon_n/2)x$ has been subtracted.

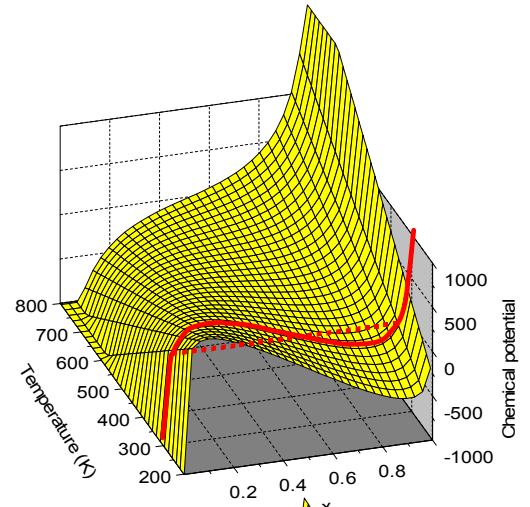
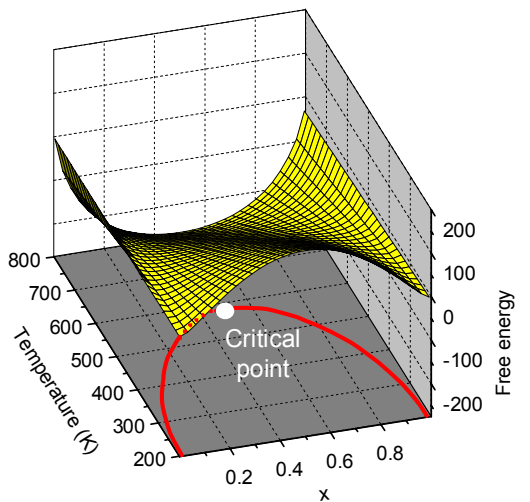
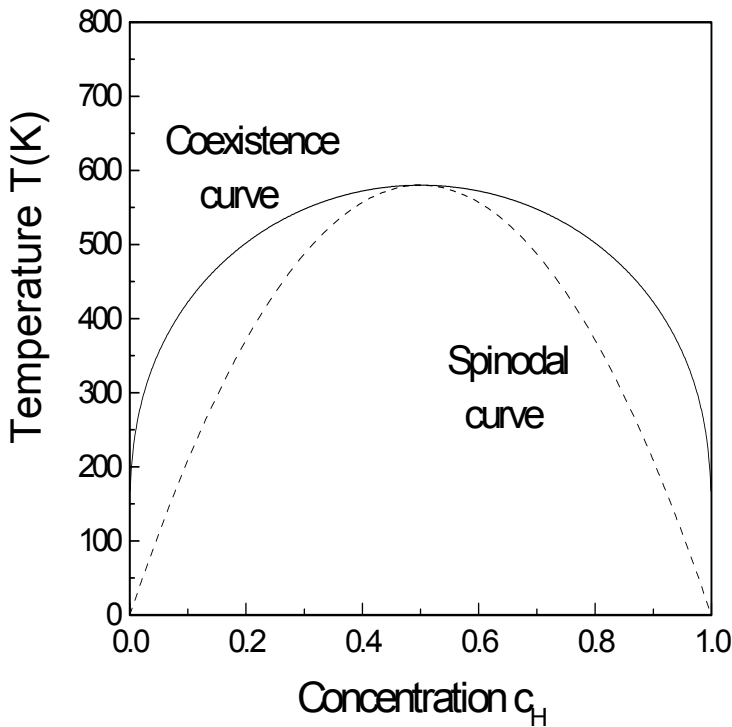
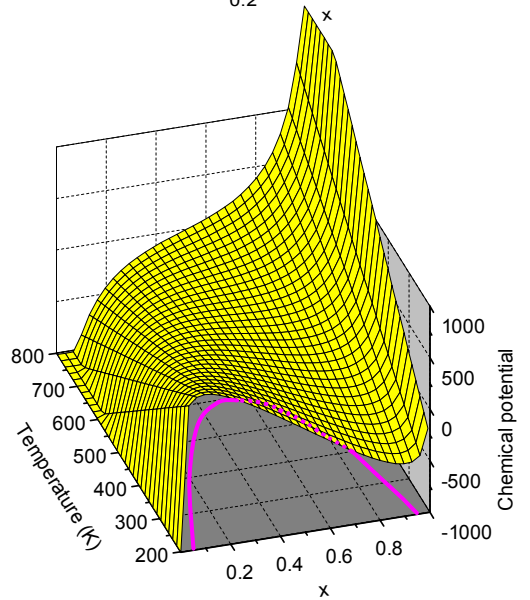


Fig. III.28: (Below) Coexistence curve and spinodal curve as determined by Eqs.III.43 and 70 for $\epsilon_n = -0.2$ eV. Note the sharp decrease in solubility of hydrogen in the metal near $c_H = 0$ and $c_H = 1$. This is very different for the spinodal curve which has a finite slope at 0 and 1.



III.3.4 INCLUSION OF THERMAL AND STERIC EFFECTS

So far we have treated the lattice-gas without taking into account that the lattice can expand (or contract) during hydrogen absorption or that the hydrogen atoms vibrate in the lattice. These effects can be taken care of in a simple way by writing,

$$\mu_H = RT \ln\left(\frac{c_H}{1-c_H}\right) + \varepsilon_0 + \varepsilon n c_H + \bar{V}_H p + \frac{3}{2} R \theta_E + 3RT \ln(1 - e^{-\theta_E/T}) \quad (\text{III.90})$$

where ε_0 , εn , and \bar{V}_H and the Einstein temperature θ_E of the lattice-gas vibrations (optical phonons) are treated as constant parameters. We then have

$$\bar{H}_H = \varepsilon_0 + \varepsilon n c_H + \bar{V}_H p + \frac{3}{2} R \theta_E + 3R \theta_E \frac{1}{e^{\theta_E/T} - 1} \quad (\text{III.91})$$

and

$$\bar{S}_H = -R \ln\left(\frac{c_H}{1-c_H}\right) - 3R \ln(1 - e^{-\theta_E/T}) + \frac{3R \theta_E}{T} \frac{1}{e^{\theta_E/T} - 1} \quad (\text{III.92})$$

and from the Gibbs-Duhem equations III.26 and 27

$$\bar{H}_M = -\frac{\varepsilon n c_H^2}{2} + \bar{H}_M^\infty \quad (\text{III.93})$$

$$\bar{S}_M = -R \ln(1 - c_H) + \bar{S}_M^\infty \quad (\text{III.94})$$

where H_M^∞ and S_M^∞ are the molar enthalpy and entropy of the pure host metal. When introduced into the Eq.III.29 for $\Delta H_{\alpha \rightarrow \beta}$ these relations lead to

$$\Delta H_{\alpha \rightarrow \beta} = \varepsilon_0 + \frac{\varepsilon n}{2} (c_\beta + c_\alpha) + \bar{V}_H p + \frac{3}{2} R \theta_E \frac{1}{e^{\theta_E/T} - 1} - \frac{1}{2} \bar{H}_{H_2} \quad (\text{III.95})$$

Since in this model $c_\alpha + c_\beta = 1$, we have that $\Delta H_{\alpha \rightarrow \beta} = H_H(c_H = 1/2)$. The slope of a $\ln p$ versus $1/T$ plot for $c_H = 1/2$ is thus continuous at the critical point.

In the low pressure regime H_{H_2} is independent of pressure and varies approximately linearly with temperature between 200 and 1000 K with a slope $\partial H_{H_2} / \partial T = 29.1$ J/K mole H_2 . This temperature variation is exactly compensated by the optical phonon term at the temperature $T_{\text{comp}} = 0.38 \theta_E$. As metal hydrides have typically $\theta_E \cong 1000$ K this implies that the temperature dependence of the last two terms in Eq.III.95 cancel each other around room temperature. For

the simple lattice-gas model considered here one thus expects the $\ln p$ versus $1/T$ plots to be linear over a large interval of temperature. For a detailed discussion of this point the reader is referred to the articles by Flanagan³⁰, Flanagan and Lynch³¹, Wicke and Blaurock, and Wicke and Brodowsky³².

To conclude this section we consider once more the case of endothermic metal-hydrogen systems. Recently, several late transition metals have been loaded with hydrogen at pressures up to 70 kbar. Unfortunately in many cases only one isotherm has been measured so that relation (1979) cannot be used for the evaluation of the heat of hydride formation. An estimate of ΔH or $\Delta H_{\alpha \rightarrow \beta}$ may, however, be obtained in the following way.

For a single-phase metal hydride the equilibrium condition (Eq.III.5) leads directly to

$$\Delta \bar{H} = T\bar{S}_H - \frac{1}{2}T\bar{S}_{H_2} \quad (\text{III.96})$$

If only half of the available sites of a given type are occupied then the mixing entropy term in \bar{S}_H vanishes. The magnitude of \bar{S}_H is therefore generally small and $\Delta \bar{H}$ is readily evaluated from the value of \bar{S}_{H_2} at a given pressure and temperature.

Similarly for a two-phase metal hydride the equilibrium conditions (Eqs.III.15 and 16) lead to

$$\Delta H_{\alpha \rightarrow \beta} = T\Delta S_{\alpha \rightarrow \beta} \quad (\text{III.97})$$

$$\Delta S_{\alpha \rightarrow \beta} = \frac{S_\beta - S_\alpha}{c_\beta - c_\alpha} - \frac{1}{2}\bar{S}_{H_2} \quad (\text{III.98})$$

$$S_i = c_i\bar{S}_H^i + \bar{S}_M^i = -R(c_i \ln c_i + (1 - c_i) \ln(1 - c_i)) \quad (\text{III.99})$$

Within the simple lattice-gas model Eq.III.98 can then be written as

$$\Delta H_{\alpha \rightarrow \beta} = -\frac{1}{2}T\bar{S}_{H_2} \quad (\text{III.100})$$

At low pressures

$$\bar{S}_{H_2} = \bar{S}_{H_2}^0 - R \ln p \quad (\text{III.101})$$

and Eq.III.100 reduces to

$$\frac{1}{2} \ln p = \frac{\Delta H_{\alpha \rightarrow \beta}}{RT} + \frac{S_{H_2}^0}{2R} \quad (\text{III.102})$$

an expression which has often been used (see for example Buschow³³) to get estimates of the heat of formation of metal hydrides with $S_{H_2}^0 = 130.8$ J/K mole H_2 .

One common feature of Eq.III.96 (with $S_H = 0$) and Eq.III.100 is that ΔH or $\Delta H_{\alpha \rightarrow \beta}$ are always negative. This seems at first sight to be in contradiction with solubility measurements in many simple metals and late transition metals (except Pd and Mn) where positive heats of solution (reaction) are found. This apparent discrepancy is easily resolved by noting that $S_H = 0$ in Eq.III.96 is not possible at infinite dilution. The discrepancy seems however to persist for concentrated hydrides of Cr, Co, Fe, Mo, and Rh for which slightly positive $\Delta H_{\alpha \rightarrow \beta}$ have been found. The explanation is that ΔH and $\Delta H_{\alpha \rightarrow \beta}$ refer to equilibrium states at a given pressure (often in the kbar range) and temperature well above room temperature. In order to reduce the enthalpies ΔH or $\Delta H_{\alpha \rightarrow \beta}$ to a chosen standard state we use the fact that

$$\bar{H}_H - \bar{H}_H^0 = \int_{p_0}^p \bar{V}_H \left(1 - \frac{\partial \ln \bar{V}_H}{\partial \ln T} \Big|_p \right) dp + \int \bar{c}_p^H dT \quad (\text{III.103})$$

where \bar{c}_p^H is the partial molar specific heat (of hydrogen in a metal) at constant pressure. It has only been measured for a limited number of metal hydrides. A direct evaluation of Eq.III.103 is thus not possible in general. The specific heat \bar{c}_p^H can, however, be estimated by means of a simple Einstein model for the optical phonons in a metal hydride. Furthermore one expects, on the basis of existing experimental data, that \bar{V}_H depends only weakly on pressure and temperature. With these approximations we find that the standard enthalpy ΔH^0 (at a suitable reference state with pressure p_0 and temperature T_0) is related to the enthalpy ΔH (at p and T) by means of

$$\begin{aligned} \Delta H^0 = \Delta H - \bar{V}_H (p - p_0) \\ - 3R\theta_E [n_{BE}(T) - n_{BE}(T_0)] + \frac{1}{2} (\bar{H}_{H_2} - \bar{H}_{H_2}^0) \end{aligned} \quad (\text{III.104})$$

where n_{BE} is the Bose-Einstein distribution function

$$n_{BE} = \frac{1}{e^{\theta_E/T} - 1} \quad (\text{III.105})$$

The Einstein temperature $\theta_E = \hbar\omega_B/k_B$ appropriate for the sites occupied by hydrogen (for octahedral sites θ_E is typically 600 K while for tetrahedral sites $\theta_E \approx 1100$ K) is assumed to be volume independent in the derivation of Eq.III.106.

Within the approximations used to simplify Eq.III.36 to Eq.III.37, the relation Eq.III.104 is valid for both ΔH and $\Delta H_{\alpha \rightarrow \beta}$. A useful form of Eq.III.104 can be obtained by combining it with Eq.III.97. We then have

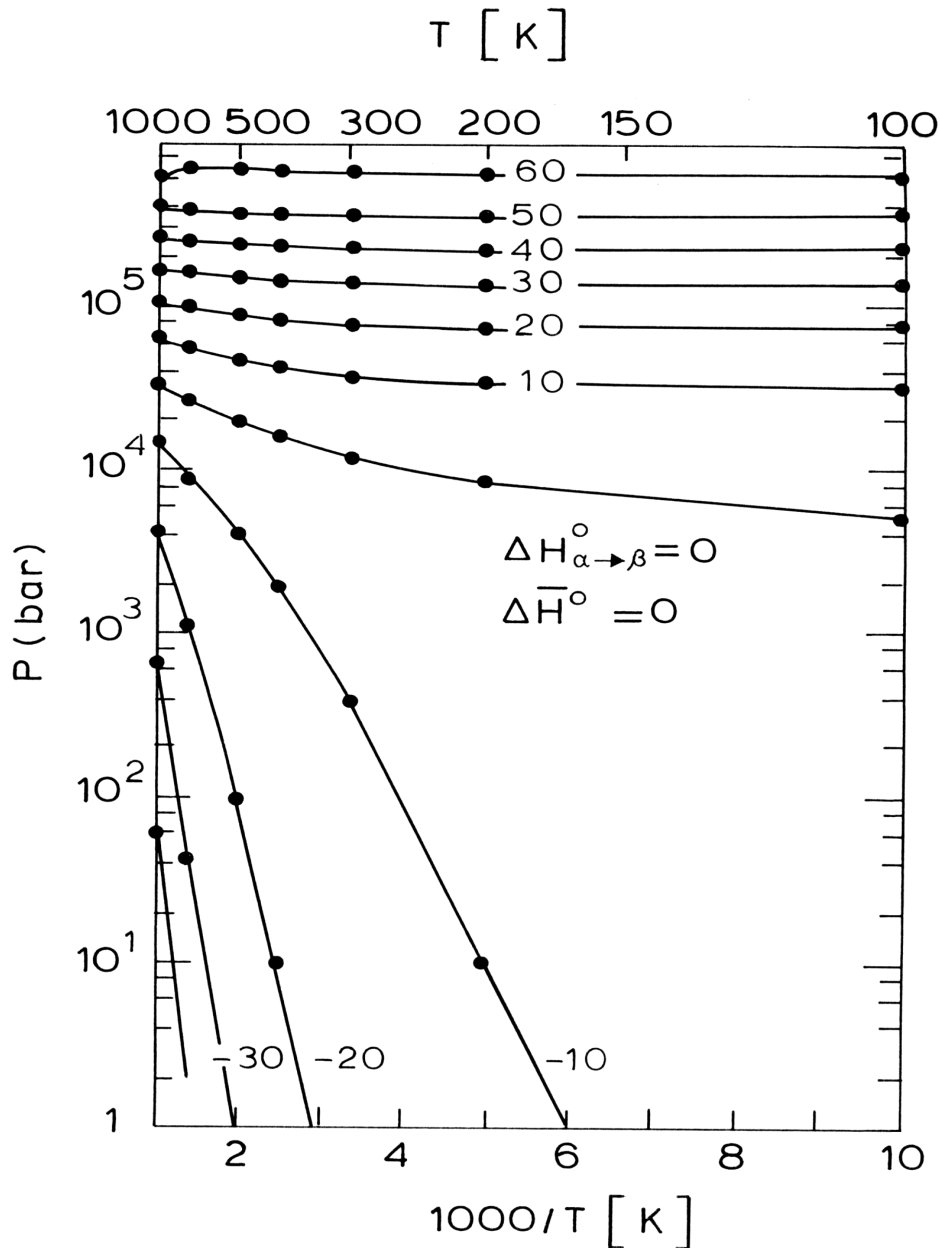


Fig. III.29: Variation of the plateau pressure with temperature for a representative metal-hydride according to relation Eq.III.90 with $\bar{V}_H = 1.7 \text{ cm}^3/\text{molH}$ and $\Theta_E = 850 \text{ K}$. For each line the standard heat of formation $\Delta \bar{H}$ is given in kJ/moleH. The values of the chemical potential of pure hydrogen are from Hemmes et al. As Eq.III.68 for $S_H = 0$ reduces to the same form as Eq.III.100 the curves shown in this figure are also valid for a single-phase metal-hydride in which only half of the sites of a given type is occupied. The number indicated in the figure correspond then to the standard heat of solution ΔH° .

$$\Delta H_{\alpha \rightarrow \beta}^0 = \frac{1}{2} \mu_{H_2} - \bar{V}_H (p - p_0) - 3R\theta_E [n_{BE}(T) - n_{BE}(T_0)] - \frac{1}{2} \bar{H}_{H_2}^0 \quad (\text{III.106})$$

At $p_0 = 1$ atm and $T_0 = 298$ K, $H_{H_2}^0 = 8.45$ kJ/mole H_2 . For a quick estimate of the standard heat of formation $\Delta H_{\alpha \rightarrow \beta}^0$ from limited high-pressure data we indicate in Fig. III.29 how $\ln p$ varies with $1/T$ at constant $\Delta H_{\alpha \rightarrow \beta}^0$ for a representative hydride (with $\bar{V}_H = 1.7$ cm³/mole H, $\theta_E = 850$ K) according to Eq.III.106. In the low-pressure regime ($p < 1$ kbar) Eq.III.106 reduces to the well-known van 't Hoff relation. At higher pressures significant deviations are observed.

With expressions of the type of Eq.III.106, Driessen et al.³⁴ determined $\Delta H_{\alpha \rightarrow \beta}^0$ for metal hydrides synthesised under high pressures. Typical values are $\Delta H_{\alpha \rightarrow \beta}^0 \cong + 5.4$ kJ/mole H for Mo, + 10 for Rh, (15 ± 2) for Co, $-(3 \pm 2)$ for Ni, $-(8 \pm 1)$ (desorption) and + 2.3 (absorption) for Cr, (10 ± 1.5) for Fe and $-(8 \pm 1)$ for Mn.

III.4 HEAT OF FORMATION OF ALLOYS

So far we have considered systems made of one type of host lattice atoms and hydrogen. The effect of alloying can often be rather important as shown in Fig. III.30 for a series of Pd-Ag alloys. Already 10 % of Ag atoms induce drastic changes in the isotherms and the corresponding two-phase region. An even more dramatic effect of alloying was found by Feenstra et al.³⁵ in an alloy of Pd containing only 5 % of uranium.

To model the absorption of hydrogen in an alloy we note that in an alloy made of A and B atoms the distribution of these atoms on the lattice sites is random. The interstitial sites which can be occupied by hydrogen are then not equivalent since they can involve various numbers of A and B atoms. For example, in a BCC alloy $Nb_{1-y}V_y$ hydrogen occupies tetrahedral sites coordinated by 4 Nb, 3 Nb and 1 V, 2 Nb and 2 V, 1 Nb and 3 V, or 4 V atoms. Each tetrahedral site is characterised by a local site energy ε_j (corresponding to ε_0 in the case of a simple lattice gas as considered in Fig. III.19). Consequently, some sites will be more favourable for hydrogen occupation than others. A simple treatment of the thermodynamics of hydrogen in an alloy can be given by noting that Eq.III.52 can be written as,

$$c_H = \frac{1}{e^{\frac{\varepsilon_0 + \varepsilon n c_H - \mu_H}{kT}} + 1} \quad (\text{III.107})$$

which resembles the well-known Fermi-Dirac statistics for electrons in a metal. The reason for the occurrence of the Fermi-Dirac statistics is due to the fact that in a lattice gas, double occupation of an interstitial site is forbidden : this is a sort of geometrical Pauli principle in real

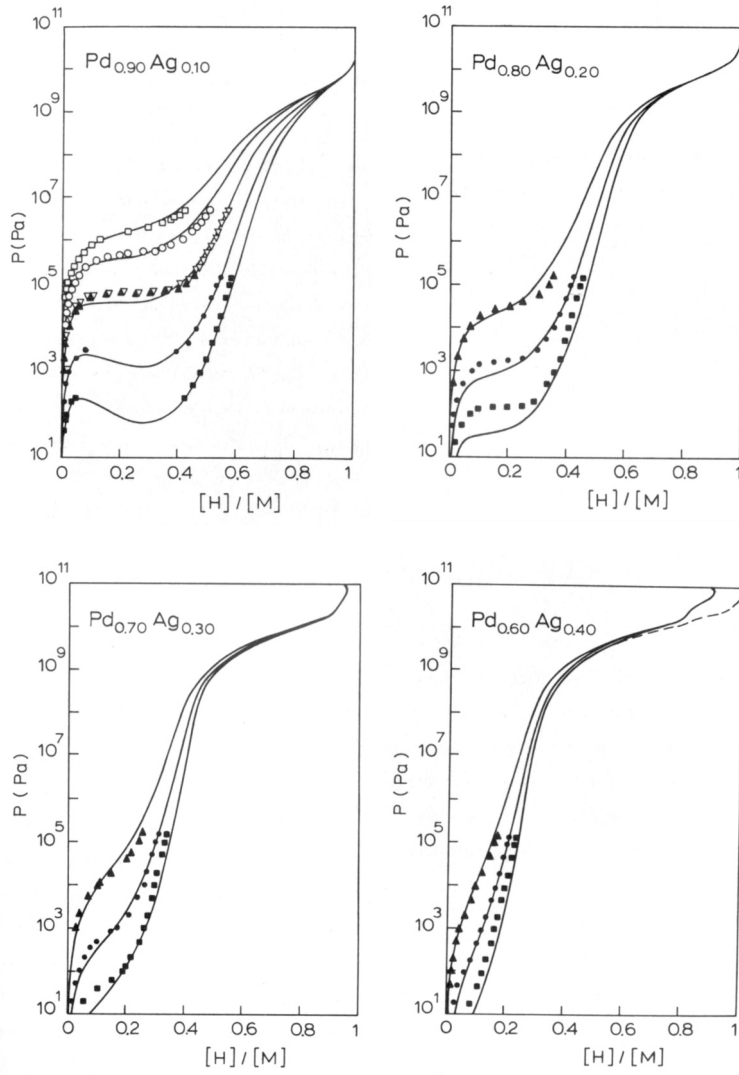


Fig. III.30: Pressure-composition isotherms for H in four Pd-Ag alloys. The dots represent measured data while the curves are calculated with a multi-site model³⁶.

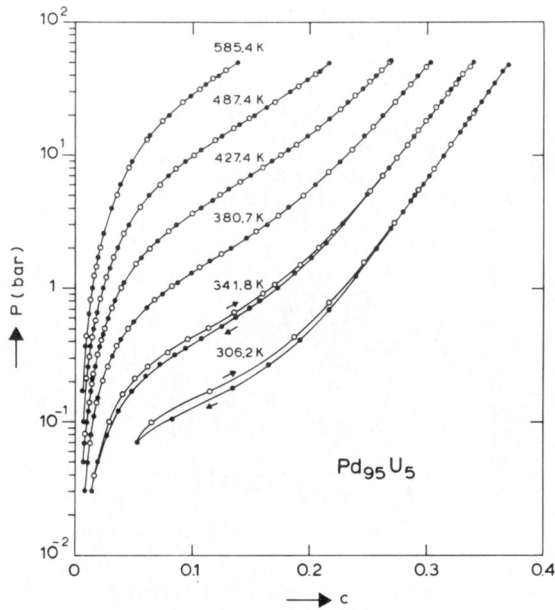


Fig. III.31: Pressure-composition isotherms for H in a Pd_{95}U_5 alloy. A comparison with the data for pure Pd (see Fig. III.2) reveals the remarkably large effect of the 5 % of uranium

space. Equation III.107 can easily be generalised to a system with a distribution of sites since at equilibrium the chemical potential of hydrogen at any site must be equal to that of hydrogen in the surrounding gas. The probability that a site j with energy ϵ_j is occupied by hydrogen is then,

$$c_H = \frac{1}{e^{\frac{\epsilon_j + f(c,T) - \mu_H}{kT}} + 1} \quad (\text{III.108})$$

in which the function $f(c, T)$ depends on the **total** concentration of hydrogen in the alloy. This assumption is reasonable since we expect the hydrogen atoms to interact elastically with each other, i.e. via long range elastic fields. The total concentration of hydrogen in the alloy is related to the local concentrations via the following relation,

$$c = \sum g_j c_j \quad (\text{III.109})$$

where g_j is the fraction of sites j in the alloy. From Eqs.III.108 and 109 one can calculate the enthalpy of formation of the alloy by means of

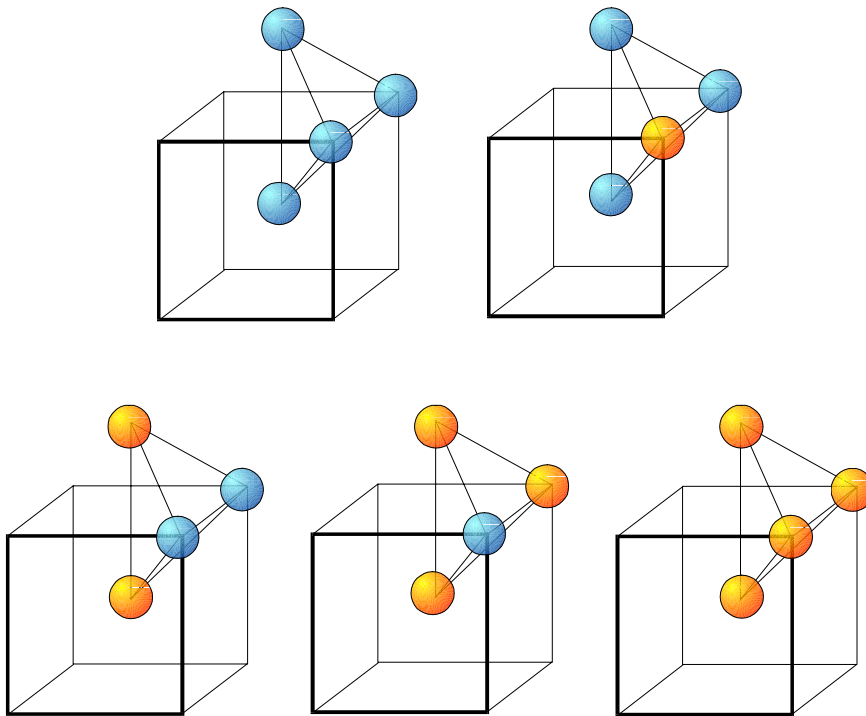


Fig. III.32: The various tetrahedral sites in an AB alloy. Each site is characterised by a different energy although the sites have the same geometry. One should note, however, that there are local distortions due the difference in size between A and B atoms. In $\text{Nb}_{1-y}\text{V}_y$ alloys it is mainly this size effect which leads to clear differences in the site energies

$$\Delta\bar{H} = h(c) + \frac{\sum g_j (1 + \cosh Z_j)^{-1} \Delta\bar{H}_j}{\sum g_j (1 + \cosh Z_j)^{-1}} \quad \text{with} \quad \Delta\bar{H}_j \equiv \bar{H}_j - \frac{1}{2} \bar{H}_{H_2} \quad (\text{III.110})$$

and

$$Z_j = \frac{\left(\varepsilon_j + f(c, T) - \frac{1}{2} \mu_{H_2} \right)}{kT} \quad (\text{III.111})$$

In Eq.III.110, $h(c)$ is the enthalpic part of the interaction $f(c, T)$ in Eq.III.108. The H-H interaction does not vary strongly from metal to metal and can be taken as the weighted average of the interaction energies in the pure AH_x and BH_x hydrides. It is then possible to determine the local

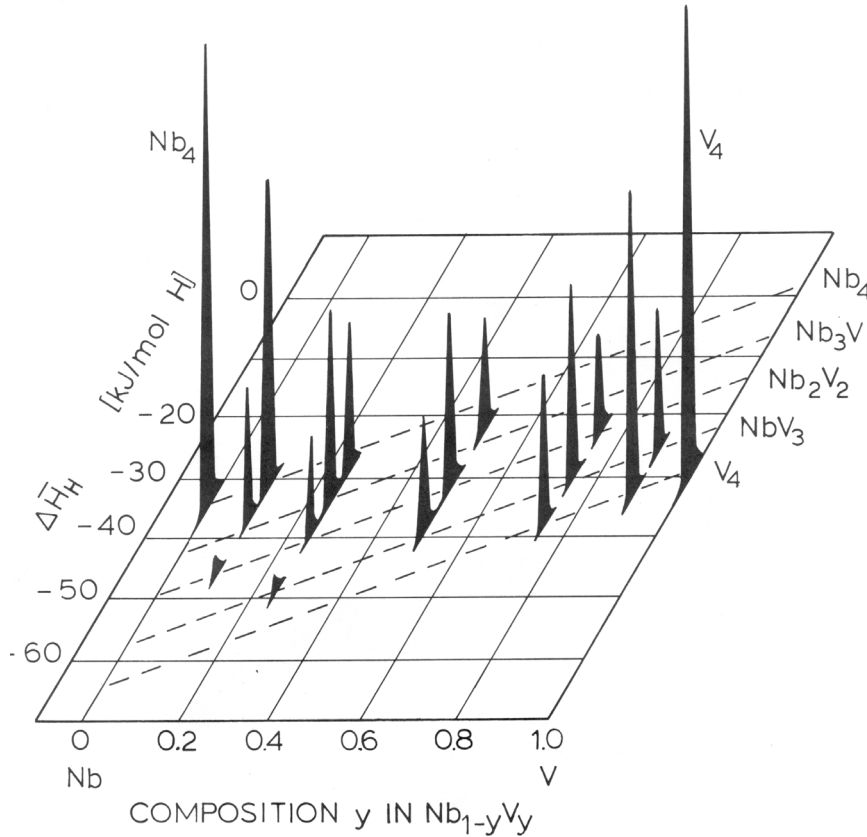


Fig. III.33: Site dependent enthalpies of solution and fraction of clusters (Nb_4, \dots, V_4) determined by Brouwer et al.³⁷ from a fit to isotherms measured by Feenstra et al on a series of $Nb_{1-y}V_y$ alloys.

enthalpies of formation ΔH_j by fitting expression III.110 to measured values of the enthalpy $\Delta\bar{H}$ (for example from measurements of pressure-composition isotherms). The result of such an approach is shown in Fig. III.33 for a series of $Nb_{1-y}V_y$ alloys. For each alloy one expects 5 δ -functions, one for each type of tetrahedral site shown in Fig. III.32. However, it is clear that in dilute alloys the fraction g_j of certain sites is too small to be considered in the fit. It is interesting to see although pure Nb and V form hydrides with essentially the same heat of formation, that

for example a V_4 cluster in a Nb rich alloy is more favourable for hydrogen than pure vanadium. This is due to the local expansion of V_4 -clusters in a Nb matrix. The reverse is observed for a Nb_4 -cluster in a vanadium matrix. It is therefore possible to use **hydrogen as a local probe for alloys**.

III.5 SEMI-EMPIRICAL MODELS

Despite the importance of ΔH , for example for technical applications, first principles calculations of the heat of formation of metal hydrides are still lacking for ternary hydrides $A_{1-y}B_yH_x$ because the theory of cohesive properties of multicomponent systems is inherently complicated and a priori calculations are still very time consuming. Until now ΔH has been calculated for selected binary hydrides MH_x only. Almost no calculations are available for ΔH in ternary metal hydrides.

The difficulty in determining ΔH from first principles has stimulated a search for empirical correlations between ΔH and physical parameters such as the unit cell volume, interstitial site size, elastic moduli, Debye temperatures and electronic specific heat. These empirical correlations are useful for the optimisation of metal-hydrogen systems for specific technical applications. In general, however, they do not provide us with more insight into the physics of hydride formation and are difficult to generalise. This is probably the reason why semi-empirical models were developed to predict ΔH for large classes of metal hydrides.

III.5.1 THE MIEDEMA MODEL

The best-known example of such a model is due to Miedema³⁸ and his collaborators. In this model each metal is characterised by two parameters (essentially the work function and the electron density at the boundary of the Wigner-Seitz cell of the elemental metal).

For the application of this model to ternary hydrides one uses the rule of reversed stability which relates, in a straightforward manner, the heat of formation of the hydride of an intermetallic compound to the heats of formation of the intermetallic compound itself and of the binary hydrides of the metals constituting the compound.

$$\Delta H(AB_nH_{2m}) = \Delta H(AH_m) + \Delta H(B_nH_m) - \Delta H(AB_n) \quad (\text{III.112})$$

The rule of reversed stability is found to work well for intermetallics made of a minority metal with high hydrogen affinity and a majority metal with a low hydrogen affinity (e.g. $LaNi_5$, YCo_5 , but not $FeTi$). For other types of compounds it generally leads to too negative values for ΔH . Several workers have tried to give a microscopic basis to the model of Miedema, but without too much success.

III.5.2 THE SEMI-EMPIRICAL BAND STRUCTURE MODEL

More recently Griessen and Driessen³⁹ proposed a semi-empirical model in which each metal is characterised by one parameter (essentially the difference between the Fermi energy and the energy of the lowest conduction band of the host metal). The heat of solution is then given by

$$\Delta H = \frac{n_s}{2} (\alpha(E_F - E_s) + \beta) \quad (\text{III.113})$$

with $\alpha = 29.62 \text{ kJ/eV/molH}$ and $\beta = -135 \text{ kJ/molH}$. In Eq.III.114 n_s represents the number of electrons per atom in the lowest s-like conduction band of the host metal. The existence of such a relation is supported by the data in Fig. III.35.

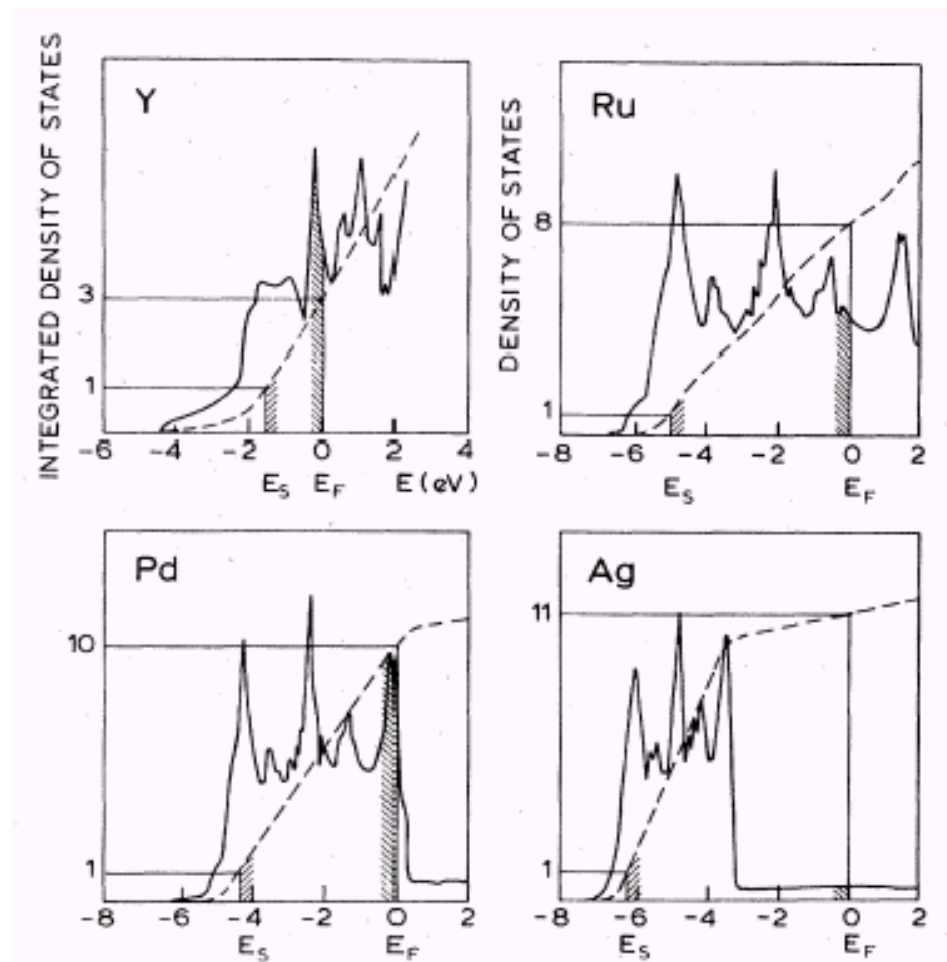


Fig. III.34: Density of states curves (full line) and the two parameters that enter the Griessen-Driessen model are the Fermi energy and an effective s-band energy E_s defined as the energy where the integrated density of states curve (dashed line) of the host metal equals 1. These parameters are indicated for three transition metals and silver. For a discussion of density of states functions, see Chapter V.

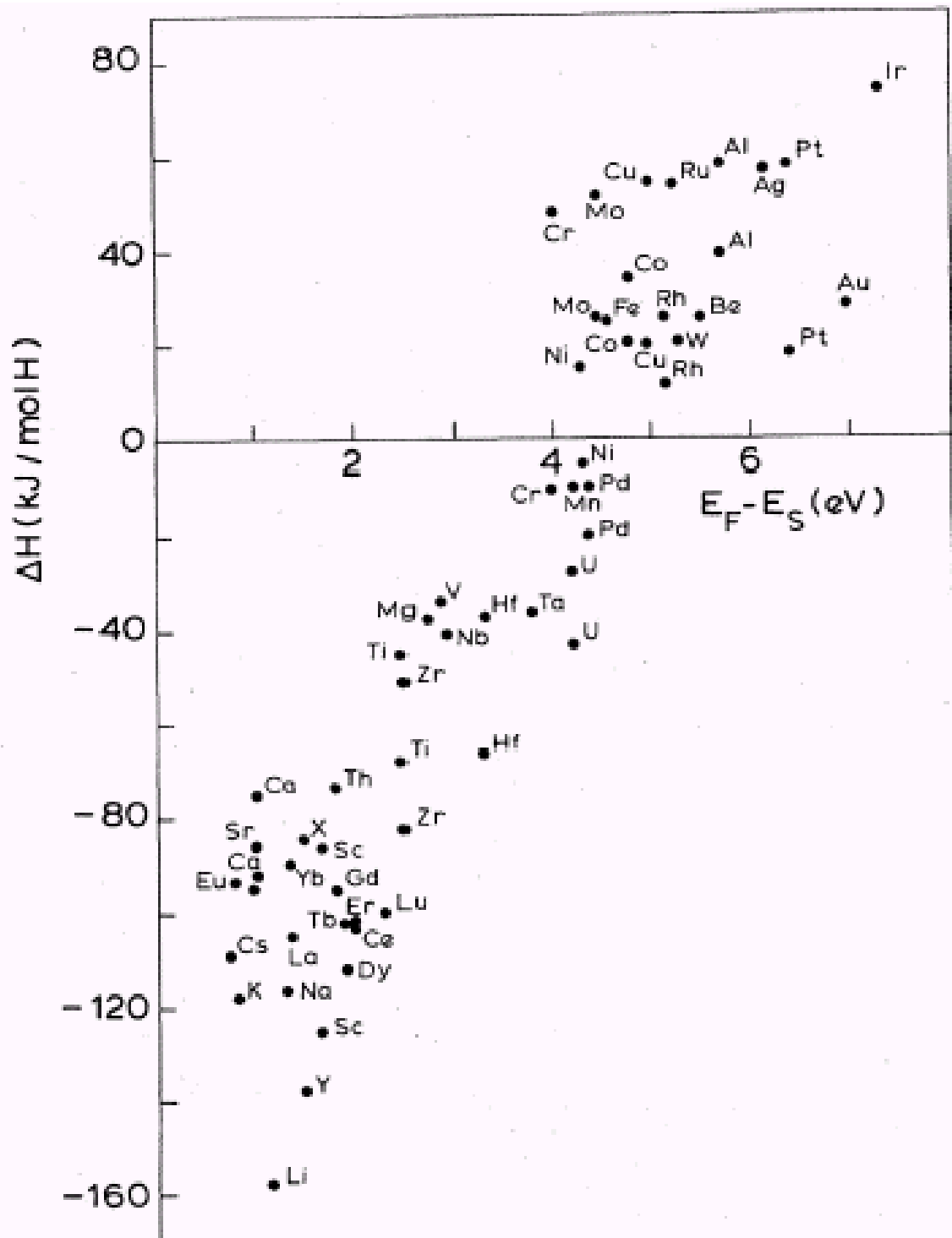


Fig. III.35: Correlation between the measured heat of formation of binary hydrides and the energy difference $E_F - E_S$ determined from existing band structure calculations for the host metal.

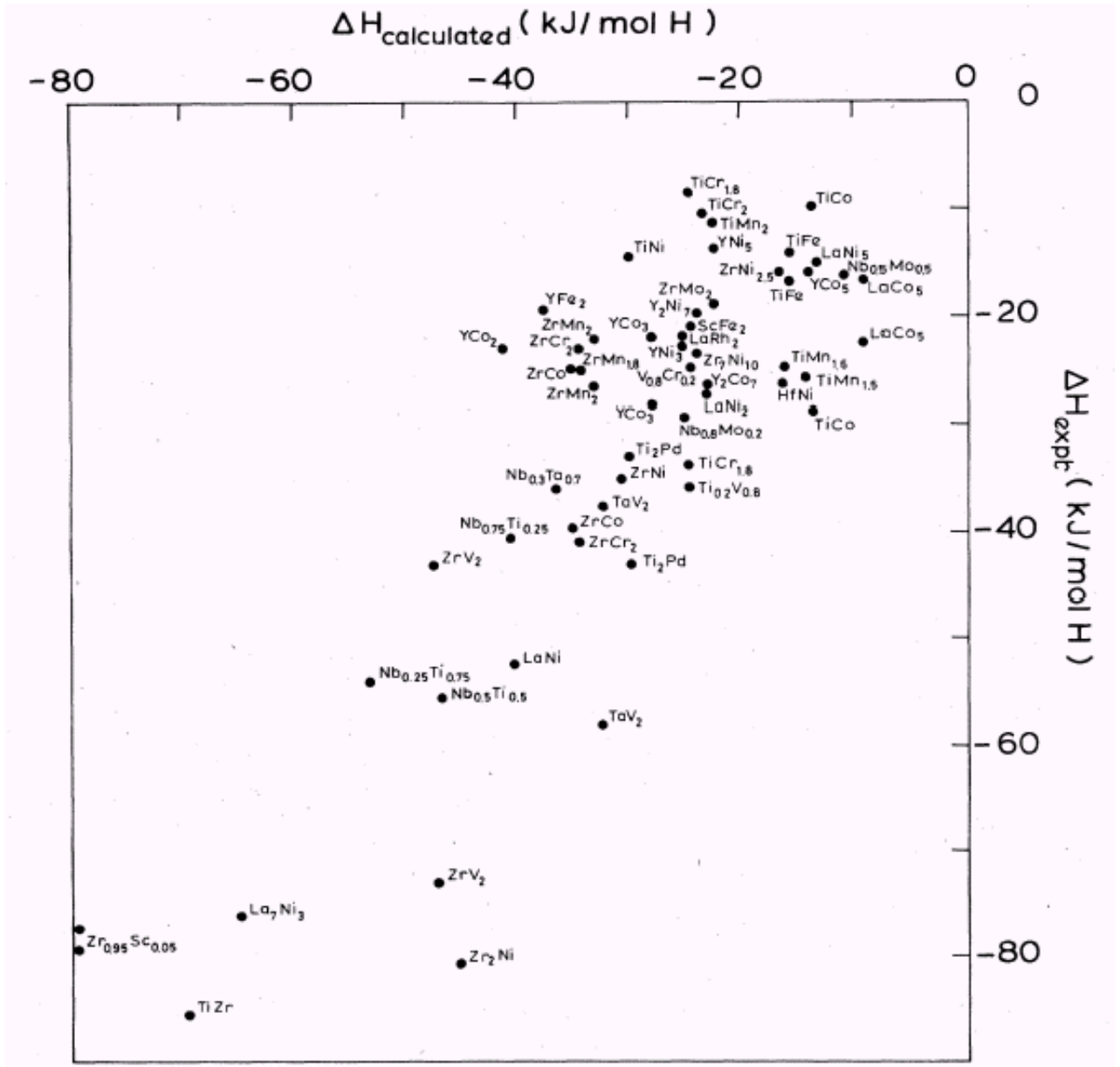


Fig. III.36: Measured heats of formation of ternary hydrides compared to the prediction of the semi-empirical band structure model. The correlation is much better than for the Miedema model.

This model reproduces well the heat of formation of binary hydrides and, when generalised to ternary hydrides, predicts ΔH values in good agreement with existing experimental data.

A generalisation of the semi-empirical band structure model that takes into account also local effects is described by Griessen⁴⁰.

III.6 REFERENCES

- ¹ Feenstra, R., R. Griessen, and D. G. de Groot, *J. Phys. F: Met. Phys.* **16** (1986) 1933
- ² Frieske, H., and E. Wicke, *Ber. Bunsengesel. Phys. Chem.* **77** (1973) 48
- ³ Gillespie, L.J., and L. S. Galstaun, *J. Amer. Chem. Soc.* **51** (1936) 2565
- ⁴ Wicke, E., and J. Blaurock, *J. Less-Common Met.* **130** (1987) 351
- ⁵ Bond, R. A., and D. K. Ross, *J. Phys. F: Met. Phys.* **12** (1982) 597
- ⁶ Pryde, J.A., and C. G. Titcomb, *Trans. Farad. Soc.* **65** (1969) 2758
- ⁷ Kuji, T., and W. A. Oates, *J. Less-Common Met.* **102** (1984) 251
- ⁸ Veleckis, E., Thesis Illinois Inst. Tech., Chicago (1960) see also Alefeld, G., *Phys. Stat. Sol.* **32**(1969) 67
- ⁹ Schober, T., and H. Wenzl, in *Topics in Applied Physics, Hydrogen in Metals II*, (ed. G. Alefeld and J. Völkl), Springer-Verlag (1978) p.11
Schober, T., and A. Carl, *Scripta Met.* **30a** (1975) 107
Schober, T., *Phys. Stat. Solidi* **30a** (1975) 107
- ¹⁰ King, H.W. and F. D. Manchester, *J. Phys. F.:Metal Phys.* **8** (1978) 15
- ¹¹ Schober, T., and H. Wenzl, in *Topics in Applied Physics, Hydrogen in Metals II*, (ed. G. Alefeld and J. Völkl), Springer-Verlag (1978) p.11
- ¹² Hill T.L., *Statistical Mechanics*, McGraw-Hill, New York (1956) and *Statistical Thermodynamics*, Addison-Wesley, New York (1960)
- ¹³ Torrey, H., *Nuovo Cimento, Suppl.* **9** (1958) 95
- ¹⁴ Alefeld, G., *Ber. Bunsenges. Phys. Chem.* **76** (1972) 335; Alefeld, G., and J. Völkl, *Hydrogen in Metals I and II*; Volumes **28** and **29** of *Topics in Applied Physics*, Springer-Verlag (1978)
- ¹⁵ Griessen, R., and T. Riesterer, "Heat of formation models" in *Topics in Applied Physics* **63** (1988) 219, Springer-Verlag
- ¹⁶ Hemmes, H., A. Driessen and R. Griessen, *J. Phys. C: Solid State Phys.* **19** (1986) 3571
- ¹⁷ Peisl, H. "Lattice strains due to hydrogen in Metals", in *Topics in Applied Physics, Hydrogen in Metals I*, (ed. G. Alefeld and J. Völkl), Springer-Verlag (1978)
- ¹⁸ Westlake, D. G., *J. Less-Common Met.* **90** (1983) 251
- ¹⁹ Bouten, P. C. P., and A. R. Miedema, *J. Less-Common Met.* **71** (1980) 147
- ²⁰ Griessen, R., and R. Feenstra, *J. Phys.* **F15** (1985) 1013
- ²¹ Feenstra, R., R. C. Brouwer, and R. Griessen, *Europhys. Lett.* **7** (1988) 425
- ²² Feenstra, R., R. Griessen, and D. G. de Groot, *J. Phys. F: Met. Phys.* **16** (1986) 1933
- ²³ Lee, T.D., and C. N. Yang, *Phys. Rev.* **87** (1952) 404 and 410
- ²⁴ Lacher, J.R., *Proc. R. Soc. London A* **161** (1937) 525; *Proc. Cambridge Philos. Soc.* **34** (1938) 518
- ²⁵ Bragg W.L., and E. J. Williams, *Proc. Roy. Soc. A* **145** (1934) 699
- ²⁶ B.H. Liu, *Encyclopedia of Materials: Science and Technology* (2001) 3953-3970 Elsevier Science Ltd (ISBN: 0-08-0431526)
- ²⁷ Wicke, E., and G. H. Nernst, *Ber. Bunsengesel. Phys. Chem.* **68** (1964) 224
- ²⁸ Simons, J.W., and T. B. Flanagan, *J. Phys. Chem.* **69** (1965) 3773
Simons, J.W., and T. B. Flanagan, *J. Chem. Phys.* **44** (1966) 3486
- ²⁹ de Ribaupierre, Y., and F. D. Manchester, *J. Phys. C: Solid state Physics* **6** (1973) L390
- ³⁰ de Ribaupierre, Y., and F. D. Manchester, *J. Phys. C: Solid state Physics* **7** (1974) 2126 and 2140
- ³¹ de Ribaupierre, Y., and F. D. Manchester, *J. Phys. C: Solid state Physics* **8** (1974) 1339
- ³² Flanagan, T. B., *J. Less-Common. Met.* **63** (1979) 209
- ³³ Flanagan, T. B., and J. F. Lynch, *J. Phys. Chem.* **79** (1975) 444
- ³⁴ Wicke, E., and H. Brodowsky, "Hydrogen in palladium and palladium alloys", (1978) in *Topics in Applied Physics, Hydrogen in Metals I*, (ed. G. Alefeld and J. Völkl), Springer-Verlag (1978) p.73
- ³⁵ K.H.J. Buschow, P.C.P. Bouten and A.R. Miedema, *Rep. Prog. Phys.* **45** (1982) 927
- ³⁶ A. Driessen, H. Hemmes, R. Griessen, *Z. f. Phys. Chem. NF* **143** (1985) 145-159.
- ³⁷ R. Feenstra, D.G. de Groot, R. Griessen, J.P. Burger and A. Menovsky, *J. Less-Common Metals* **130** (1987) 375-386.
- ³⁸ H. Hemmes, E. Salomons, R. Griessen, P. Sanger, A. Driessen, *Phys.Rev.B* **39** (1989) 10606-10615.
- ³⁹ R. Feenstra, R. Brouwer, R. Griessen, *Europhysics Letters* **7** (1988) 425-430.
- ⁴⁰ Miedema, A. R., K. H. J. Buschow, and H. H. van Mal, *J. Less-Common Met.* **49** (1976) 463
- Griessen, R., and A. Driessen, *Phys. Rev.* **B30** (1984) 4372
- Griessen, R. *Phys. Rev.* **B38** (1988) 3690-3698